DESIGN AND OPTIMIZATION OF A FAST-NEUTRON, EXTERNALLY DRIVEN THORIUM-LITHIUM-BERYLLIUM FLUORIDE MOLTEN SALT SUBCRITICAL ASSEMBLY

A Thesis

by

CRISTIAN OLIVER GARZA

Submitted to the Office of Graduate and Professional Studies of
Texas A&M University
in partial fulfillment of the requirements for the degree of

MASTER OF SCIENCE

Chair of Committee,	Sean McDeavitt
Co-Chair of Committee,	Sunil Chirayath
Committee Member,	Michael Pate
Head of Department,	Michael Nastasi

December 2020

Major Subject: Nuclear Engineering

ABSTRACT

An externally driven subcritical molten FLiBe-Thorium LiF-BeF_2-ThF_4 (52.8-27.2-20 mol%) salt assembly is being constructed at Texas A&M Nuclear Engineering and Science Center (NESC). The experiment is called the Thorium Engineering and Science Assembly (ThESA). The objective of ThESA was to be a separate effects test to isolate the phenomenon of thorium-232 fissioning in a FLiBe medium. ThESA was chosen to be driven with a deuteron-deuteron generator to ensure an unobscured fission neutron flux above the 3 MeV threshold. It was the objective of this thesis to support the design of ThESA to ensure the maximization of thorium fissioning in a FLiBe medium. The thesis work was initiated with a comparison study between differing pin and pool assembly types. Multiple pins and pool type assemblies were analyzed using MCNP with either FLiBe-Th or a combination of FLiBe and ThO_2 to measure the effective neutron multiplication factor (k-inf), neutron flux, and fission rates. The comparison study included each design's practicality, such as fuel heating, transportation, and glovebox physical restraints, as well as neutronics results. The results of the comparison study indicated that a pool-type would be the superior choice in producing the most thorium fissions in FLiBe. The pool-type assembly was also the most experimentally practical considering design and operational constraints. Following the final assembly choice, a parametric reflector study was performed on the pool type assembly. The reflector study results indicated that the ThESA objective would not benefit from a reflector, considering a large and heavy reflector's cost and complexity. After the mechanical team matured the design, a safety analysis was performed that included dose

rates, criticality simulations, and an assessment to ensure no proliferation threats. The safety analyses revealed no significant hazards from ThESA. Then the addition of steel inserts in the pool intended for data gathering equipment was included in the MCNP model. The inclusion of the steel inserts was done to ensure that there would not be a significant reduction in the thorium fission rate. The analysis revealed that steel inserts would not induce a meaningful reduction in the assembly's fission rate. The final study goal was to capture the energy dependent neutron flux spectrum to capture the fraction of fission neutrons that, with certainty, would be differentiable from the source neutrons. The flux was subdivided into energy groups to observe the neutrons born from fission with energies above 3 MeV. The 3 MeV threshold was chosen due to the lack of source neutrons above this energy range. The total neutrons produced from fission above 3 MeV was 2.87E5 +/- 5.75E+01 neutrons per second. The work performed in this study did reveal that there was a substantial fission neutron population that could be differentiated from the source neutrons to be studied in an isolated effects test.

DEDICATION

This document is dedicated to my parents Silvia and Oliver Garza, who filled me with the desire to reach for the stars. They transplanted their lives from Mexico to the USA to ensure I would have the freedom and opportunity to chase my dreams. Also, to my dear grandmother, who unfortunately passed shortly before the completion of this thesis. I only hope that I've honored you within my pursuits. Anything ever done has only been done with the help and support of loved ones. To my loved ones, I say thank you.

ACKNOWLEDGEMENTS

I would like to thank my committee chair and co-chair, Dr. McDeavitt and Dr. Chirayath, for their guidance and support throughout this research. I would like to thank my dear friends, peers, and the Department of Nuclear Engineering for making my time at A&M a wonderful experience. Thanks also to my loving father and mother, who encouraged me to reach for greater and greater heights. I would also like to thank my Fiancé for having supported me mentally and emotionally during my academic studies.

CONTRIBUTORS AND FUNDING SOURCES

Contributors

This work was supervised by a thesis committee consisting of Professor McDeavitt and Professor Chirayath of the Department of Nuclear Engineering and Professor Pate of the Department of Mechanical Engineering. I would also like to acknowledge Allen Jorgensen and David Stout for assisting with FLiBe-Th material card calculation. I would like to thank Dr. Chirayath for assisting with troubleshooting in MCNP. Your experience and direction were invaluable to the project.

Funding Sources

Graduate study was supported by a grant from Texas Thorium, LLC.

NOMENCLATURE

FLiBe-Th	$LiF\text{-}BeF_2\text{-}ThF_4$ (52.8-27.2-20) mol %
NESC	Texas A&M Nuclear Engineering and Science Center
ThESA	Thorium Engineering and Science Assembly
MSRs	Molten Salt Reactors
ThO_2	Thorium-Dioxide
SS304	Stainless Steel 304
ZrS	Zirconium-Silicide
LFTR	Liquid Fluoride Thorium Reactor
LWR	Light Water Reactor
MCFR	Molten Chloride Fast Reactor
CAD	Computer Aided Design Model
DD	Deuteron-Deuteron
k-eff	The effective neutron multiplication factor
k-inf	The effective neutron multiplication factor in an infinite medium
ENDF	Evaluated Nuclear Data Files
JANIS	JAVA Based Nuclear Data Information System

TABLE OF CONTENTS

Page

LIST OF FIGURES

Page

LIST OF TABLES

Page

1. INTRODUCTION

1.1. Overview

This document's computational simulations were performed to support the design and construction of a fast-neutron externally driven LiF-BeF_2-ThF_4 (52.8-27.2-20) mol % (FLiBe-Th) subcritical assembly. This work is part of a larger molten salt reactor (MSR) program at Texas A&M University funded by Texas Thorium, LLC (Houston, TX). The thorium research initiative has two principal components: 1) establishing a fast, subcritical system for separate effects experiments and 2) developing MSR technology and methods through the construction and operation of a thermal-hydraulics experiment loop (not part of this work).[1] The MSR technology component is a complementary but separate part of the Texas Thorium research initiative and will not be described further.

The subcritical system has been named the Thorium Engineering and Science Assembly (ThESA). There are three primary tasks in the ThESA project: 1) computational simulations to guide design decisions for the system, 2) design, fabrication, and installation of the ThESA components and 3) establish salt halt handling, purification, and mixing equipment and methods to prepare the ThESA salt.

The computational simulations are presented here and completed first, whereas the last two tasks are still underway as the ThESA system is assembled[1].

1.2. Project Outcome

A thorough simulation of the ThESA was created to enable design decisions in MCNP. Chapter 3 covers the methodology used to simulate ThESA in MCNP. Chapter 4 presents a comparison study between pin and pool type assemblies filled with varying materials. The comparison study was performed between a pure FLiBe-Th pin set, a FLiBe-Th mix thorium-dioxide-(ThO_2) filled pin set, and a FLiBe-Th pool type assembly. The assembly-type study also considered the practicality of the assembly types as well as the neutronics results. The comparison study concluded that the pool type would produce the most neutrons from specifically thorium fissioning in a FLiBe medium. Secondly, the pool type would be the most experimentally practical to design and operate. Chapter 5 describes a parametric reflection study that compared the benefits of a large stainless steel 304 (SS304) and a zirconium silicide (ZrS) reflector. The parametric reflector study concluded that a reflector would have added unnecessary cost and complexity for insignificant increases in the thorium fission rate. Chapter 6 presents a safety analysis of the ThESA design, examining the dose rates, unintended accidental criticality events, and accessing whether there were any proliferation threats posed by ThESA. The safety analyses revealed that ThESA could be operated safely outside of the

[1] The ThESA team is led by Dr. Sean McDeavitt and incudes Drs. Delia Perez-Nunez and Luis Ortega as research leads with Cristian Garza (Task 1), Elohi Gonzalez (Task 2), Richard Livingston (Task 3), T. David Stout (Task 3), and Allen Jorgenson (Task 3).

experimental room; the assembly could not reach accidental criticality and did not produce significant uranium-233 or tritium quantities. Chapter 7 described the evaluation of the effects of the accessory pipes' addition on the fission rate and simulated the flux spectrum to isolate the fission neutron spectrum. Chapter 7 concluded by identifying the total fission neutrons produced throughout the pool assembly.

2. BACKGROUND AND LITERATURE REVIEW

2.1. Thorium as a Nuclear Fuel

Over the last decade, there has been renewed interest in developing and commercializing molten salt reactors.[2] Some MSR variants, like the Liquid Fluoride Thorium Reactor (LFTR), use thorium instead of natural uranium for the fertile component. The primary benefit of using thorium is that it can exclusively produce fissile material with thermal neutrons, avoiding a hardened spectrum's inherent technical challenges.[3] Thus, it has an enormous potential to be used as a fuel additive alongside fissile material to increase fuel burnup. The added fuel burnup is due to the thorium-232 advantageous ability to produce additional fuel via uranium-233 production.[4] Thorium is also found in greater abundance by a factor of three in the earth's crust than natural uranium. [5] Along with a higher natural abundance and the ability to extend fissile material inventory, it increasingly makes thorium an attractive nuclear fuel.

ThO_2 in Light Water Reactors (LWR) has significant material characteristic advantages over UO_2 shown in Table 1. Firstly, it is a remarkably nonreactive solid and is one of the most refractory materials.[6] Secondly, ThO_2 has a higher melting point than UO_2. ThO_2 does not oxidize any further passed the one-two stoichiometric ratio it exists in. Modification of the stoichiometry may have unintended effects on thermal gradients, fuel clad interactions, and neutronics properties. Subsequently, ThO_2 has a higher thermal conductivity, which ensures a lower operating temperature, leading to a decrease in the coolant velocity or an increase in the coolant's thermal output temperature. ThO_2 is also less prone to thermal expansion compared to UO_2, making it less prone to fuel-clad

interactions.[6] Although ThESA is not focused on ThO_2 specifically, it is relevant that the neutronics properties of thorium-232 are well understood to ensure the successful deployment of this alternative nuclear fuel.

Table 1. The properties of ThO_2 that are superior compared to UO_2.[6]

Properties	**UO2**	**ThO2**
Thermal conductivity (W/m-°C)	8.0	10.3
Melting Point (°C)	2850	3650
Thermal Expansion (μm/m°C)	9.8	8.9

Thorium-232 has passive proliferation resistance as in addition to uranium-233, uranium-232 is also produced. If uranium-233 material were diverted from an LFTR seed blanket, there would be significant uranium-232 contamination producing high energy gamma radiation.[7] The subsequent uranium-232 contamination would make a diversion arduously complicated and dangerous.[7]

Furthermore, the thorium-232 life cycle has improved waste characteristics as nuclei with atomic mass below 235 cannot produce actinides such as neptunium, americium, curium, and plutonium. [8] Figure 1 shown below displays the composition of actinides produced from uranium fissioning that would not be present in the thorium life-cyle.

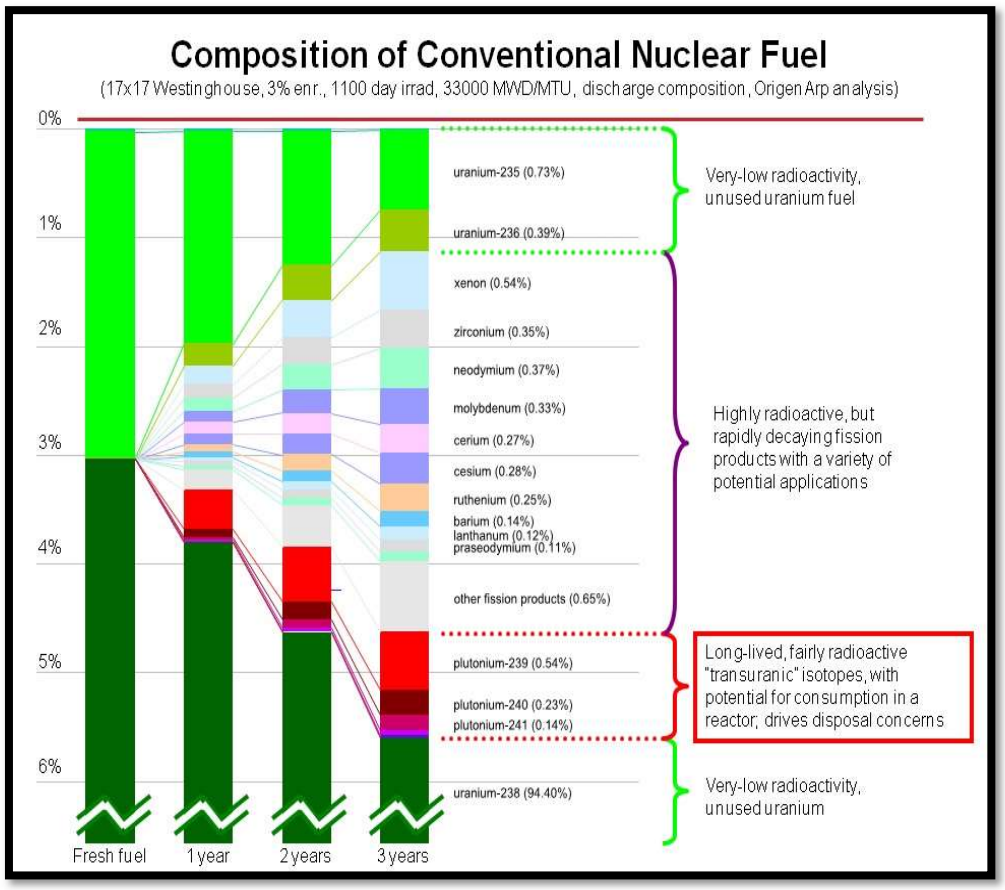

Figure 1. The waste composition of standard UO_2 after a three-year use cycle (Kageneck, 1998).[10]

Using thorium instead of uranium, the removal of actinides in nuclear waste leads to a reduction in radiotoxicity on the order hundreds and thousands of years shown in Figure 2. Although nuclear waste would still be dangerously radioactive due to fission products, most of the relative radiotoxicity would be diminished on the timescale of hundreds of years.[11]

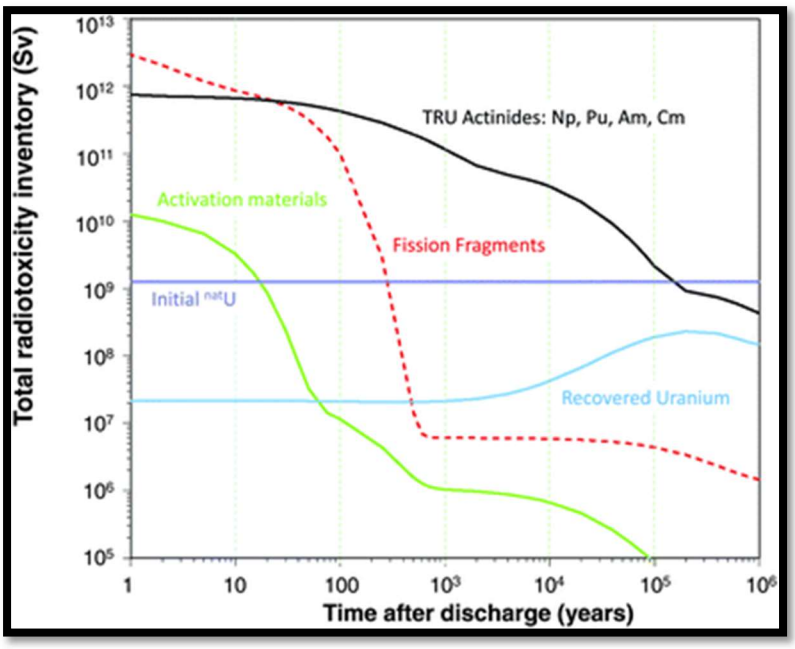

Figure 2. The radiotoxicity inventory of once-through UO_2 fuel as a function of time (Colonna, 2010) .[11]

2.2. Relevant Nuclear Reactor Systems

ThESA is a subcritical assembly with FLiBe-Th fuel salt and driven by external high-energy source neutrons. Unlike other subcritical assemblies, ThESA has no fissile driver but consists of only fertile thorium-232 homogenized into a FLiBe salt. The FLiBe salt in ThESA is like that of the seed blanket surrounding an LFTR, a variant of an MSR. A seed blanket is an external fertile infused salt blanket surrounding an LFTR's primary core. A full LFTR plant diagram is shown in Figure 3. ThESA shall mimic the seed blanket as it is composed of a similar salt medium with a thorium fuel blended in. The principal mission of the ThESA system is to elucidate understanding of the

neutronic impacts on a FLiBe-Th salt exposed to an external neutron flux. ThESA is driven by an external high-energy neutron generator that directly fissions the fertile thorium-232 in the FLiBe. The fast neutron spectrum mimics the degenerative effects that fast neutrons can have on a fertile mixed FLiBe-Th salt.

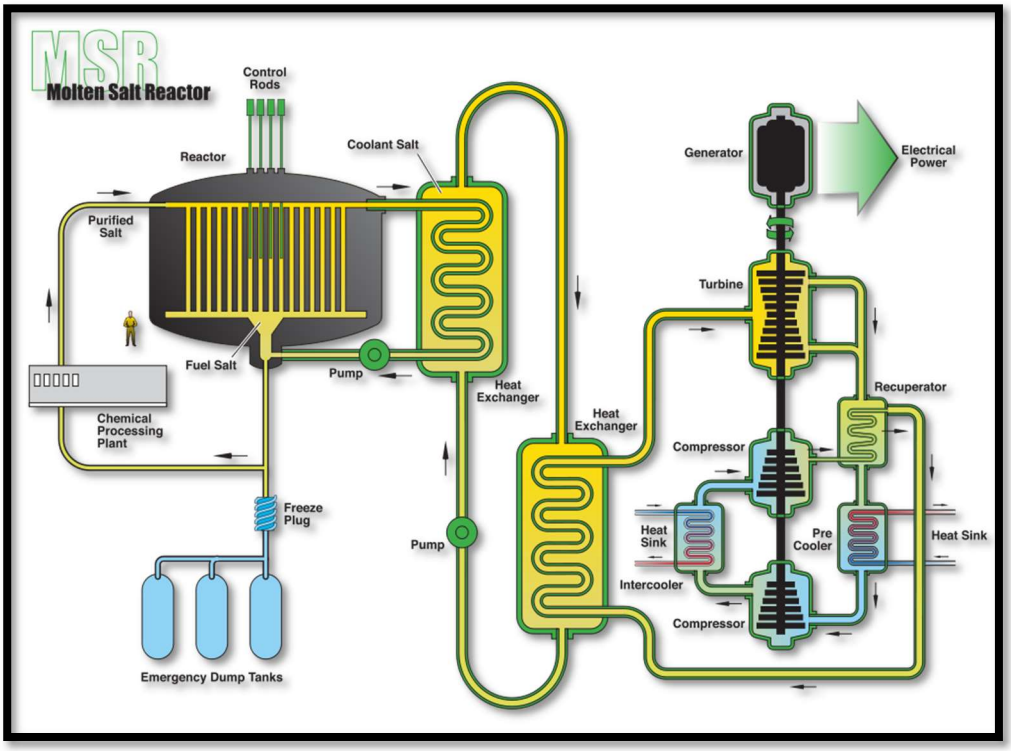

Figure 3. An LFTR full-plant diagram (Juhasz, 2009).[12]

Similarly, Accelerator Driven Systems (ADS) was reviewed since ThESA is also an externally driven system. Understanding the technical challenges faced by ADS can potentially shape ThESA design to understand systems with external drivers thoroughly.

2.2.1. Molten Salt Systems

As discussed previously, understanding the neutron interactions and seed blanket degradation in a high neutron flux is critical to the operation of MSRs. Thus, understanding the history and development of MSRs is also valuable. The development of MSRs began to meet the needs of long-range supersonic nuclear bombers, emphasizing extended operational times. Thus, was born the Aircraft Nuclear Propulsion (ANP) program that directly led to the Aircraft Reactor Experiment (ARE). The ARE was a sodium-cooled ZrF_4-UF_4 molten salt reactor that achieved criticality for a total of 221 hours, shown in Figure 4.[13] The ARE proved the concept that liquid fuel could achieve sustained controlled nuclear fission.

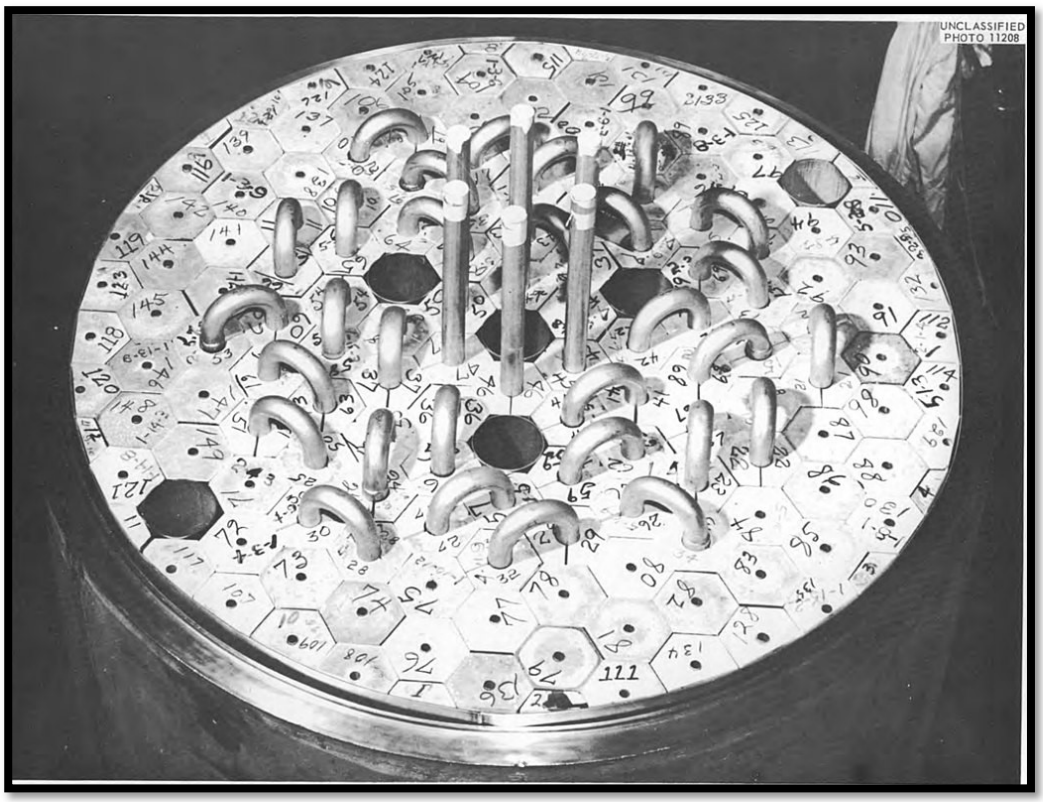

Figure 4. The aircraft reactor experiment with the interlaced fuel tubes in BeO blocks (Ergen, 1957).[14]

After the ARE concluded, the technical experience was transferred to the Molten Salt Reactor Experiment (MSRE).[15] The MSRE mission was to demonstrate the safe operation of an epithermal thorium breeder reactor. The MSRE mission determined if the neutronics kernel at the core of an LFTR could sustain criticality and prove a reliable and straightforward reactor.[15] The MSRE was fueled using LiF-BeF_2-F_4-UF_4 (65.0 - 29.1-5.0-0.9 mol%), a variant of salt that ThESA will use with the exception of uranium and slightly different mol percentages.[16] Figure 5 shows the critical salt characteristics of the fuel salt used in the FLiBe.

Fuel Salt		
Composition:	^{7}LiF-BeF_2-ZrF_4-UF_4 (65.0-29.1-5.0-0.9 mole%)	
Properties at 1200°F (650°C)		
Density	141 lb/ft^3	2.3 g/cm^3
Specific heat	0.47 Btu/lb-°F	2.0×10^3 J/kg-°C
Thermal conductivity	0.83 Btu/h-ft-°F	1.43 W/m-°C
Viscosity	19 lb/h-ft	29 kg/h-m
Vapor pressure	<0.1 mm Hg	$<1 \times 10^{-4}$ bar
Liquidus temperature	813°F	434°C
Coolant salt[a]	^{7}LiF-BeF_2 (66-34 mole%)	
Moderator	Grade CGB graphite	
Salt containers	Hastelloy-N (68 Ni-17 Mo-7 Cr-5 Fe)	
Cover gas	Helium	

Figure 5. The FLiBe salt characteristics for the MSRE (Haubenreich, 1970).[16]

The MSRE contained a large cylindrical graphite matrix with fuel channels that moderated the fissile material to induce nuclear fission in the primary vessel shown in Figure 6. The MSRE operated for over 9000 full power hours using uranium-235.[16] Alternatively, MSRE was the first nuclear reactor to reach criticality with uranium-233, which is the byproduct of the thorium neutron bombardment. The MSRE successfully operated on the thorium-based fissile material for 2500 equivalent hours.[16]

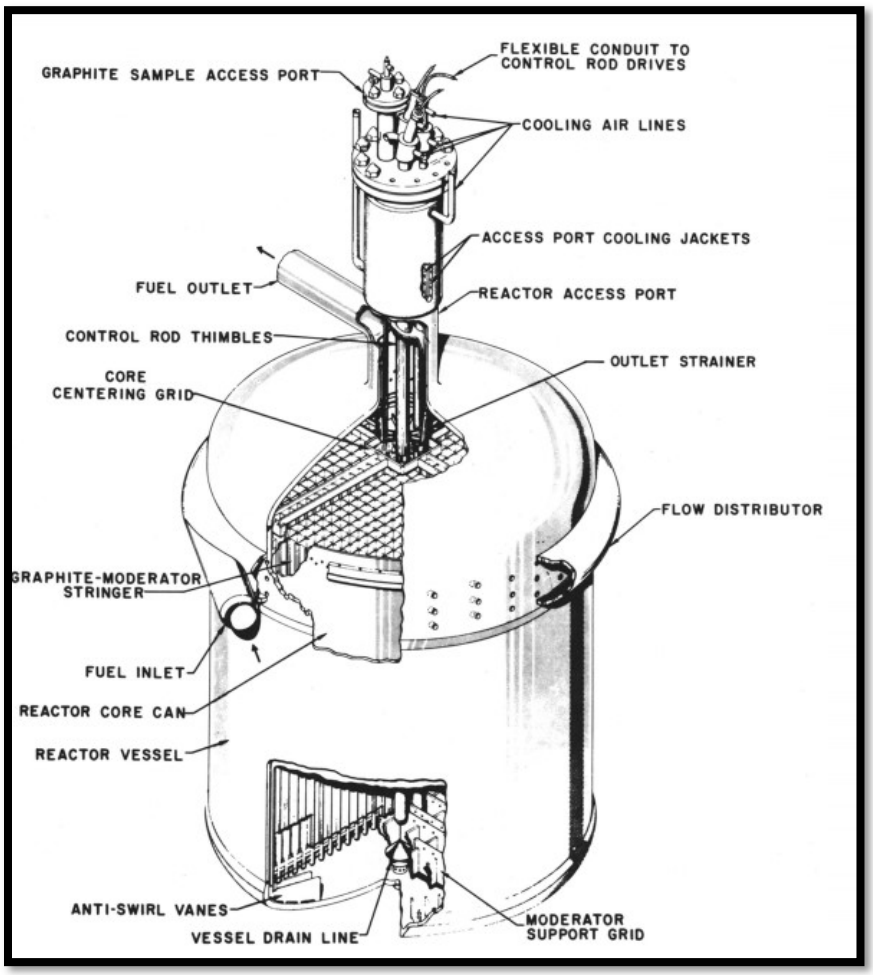

Figure 6. The MSRE core diagram with the channeled graphite moderator matrix (Haubenreich, 1970).[16]

A full-scale version would have contained the thorium seed blanket that would have produced additional fuel. The MSRE was a significant success, proving that an MSR can operate for extended periods of time. Additionally, maintenance can occur safely without extended delays, and it provided valuable nuclear characteristics for the

nuclear scientific community. The ThESA core seeks to gain valuable insight into the neutron interactions occurring within a FLiBe-Th blanket proposed in LFTR systems.

2.2.2. Accelerator Driven Systems

There are several variants of Accelerator Driven Subcritical System (ADS) type reactors that have proposed using the thorium fuel life cycle to produce uranium-233 to be burned in core or used as a means to seed other next-generation fast neutron spectrum reactors. Thus, similar to LFTRs, it is essential to understand thorium's neutronics in a medium with an externally driven system. Figure 7 shown below displays an example of the full plant system that an ADS reactor would use.

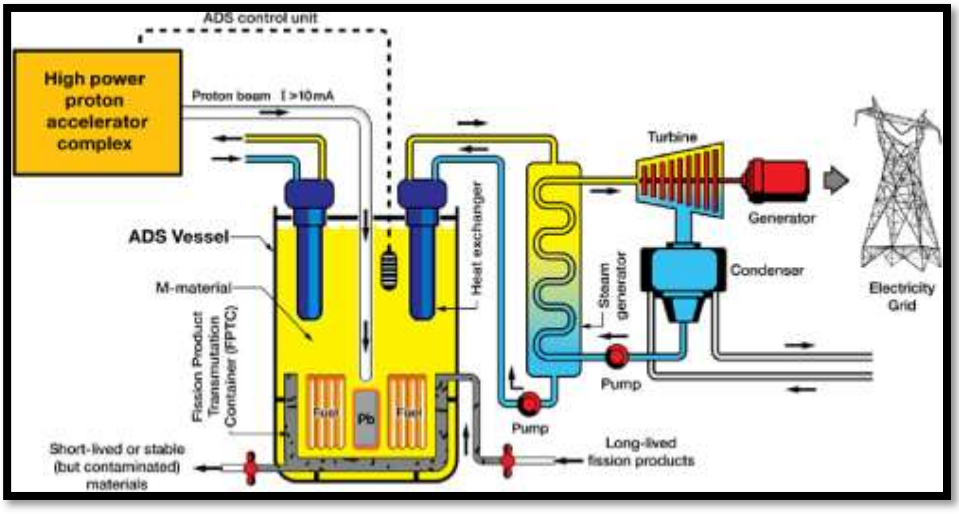

Figure 7. A proposed plant configuration using the ADS system (Glass, 1998).[17]

ADS reactors have a neutron multiplication factor (k-eff) less than 1.0;[18] thus cannot have a sustained fission chain reaction independently. Consequently, a particle accelerator is used to increase the protons to several MeV or GeV, which collide with a high Z material such as tungsten, lead, lead-bismuth, or mercury located at the center of the ADS core. High energy protons collide with one of these materials lead to excitation, and the resulting deexcitation releases neutrons. The resulting neutrons can then produce fission directly or indirectly through the production of additional fissile material. An ADS system can be built with a combination of thorium-232 and reprocessed fuel doped with spent fuel, as shown in Figure 8. The ADS core with thorium-232 and reprocessed fuel would not need additional uranium-233 enrichment and could reach a subcritical k-eff between 0.90 ~0.98.[19] The high k-eff is due to the plutonium and uranium-235 in the reprocessed fuel and the removal of neutron poisons. The system would be viable and produce uranium-233 without additional enrichment. A system with this configuration would increase the uranium-233 while simultaneously reducing actinide and plutonium in the spent reprocessed fuel.

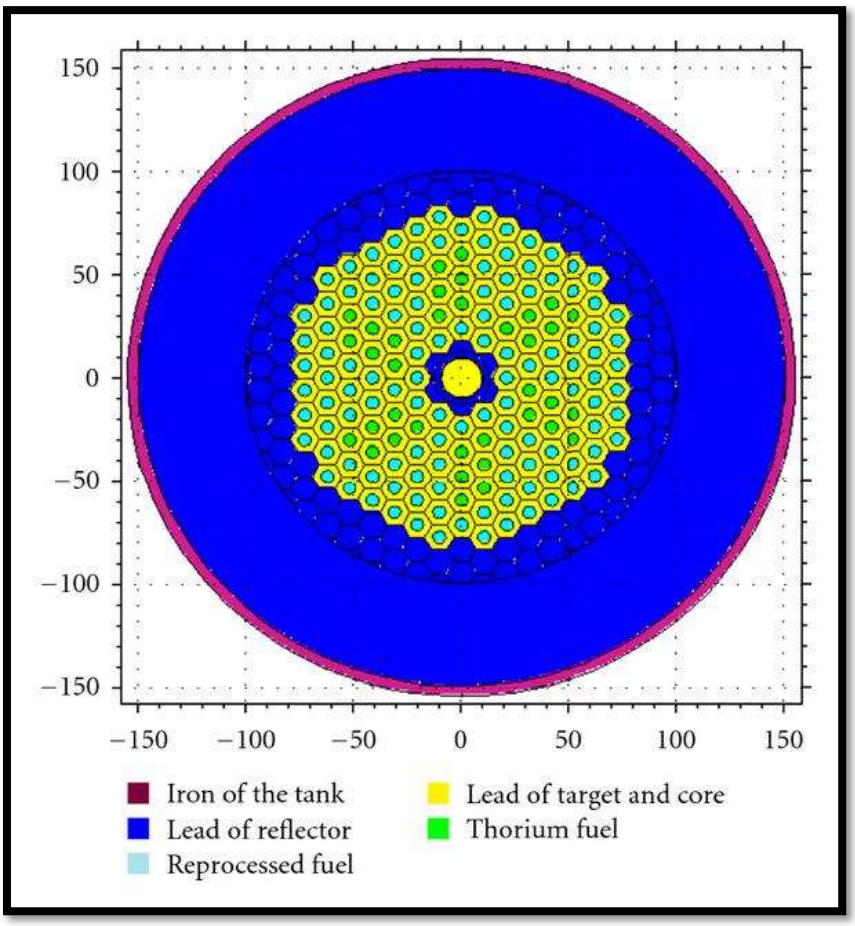

Figure 8. An ADS core with thorium and reprocessed fuel (Bowman, 1998).[19]

Although ThESA is not driven using neutron spallation via a proton source, it can still be valuable to understand how a subcritical thorium fueled systems may react to external neutron sources.

2.2.3. Active Molten Salt Projects

There are several active molten salt projects in the US, Canada, and the Netherlands.[20] TerraPower, located in the US, is developing a Molten Chloride Fast

Reactor (MCFR). MCFR will be a prototype commercial reactor used to prove the economic and technical practicality of molten chloride fast spectrum reactors. The MCFR's power output will be in the range of 30-150 MW_{th}. Figure 9, shown below is TerraPower MCFR. The reactor will use a highly enriched fissile seed for the startup.[21] After startup, the reactor will act as a net breed-burner, meaning it will produce as much fuel as it consumes over its lifetime. The MCFR will require the addition of either depleted uranium or natural uranium to continue operation. MCFR will be equipped with online reprocessing to remove neutron poisons and reduce downtime. MCFR was chosen to be a chloride based on the neutron spectrum's hardening to ensure maximum fuel burnup. Construction is expected to begin on the demo MCFR around 2025-2027.

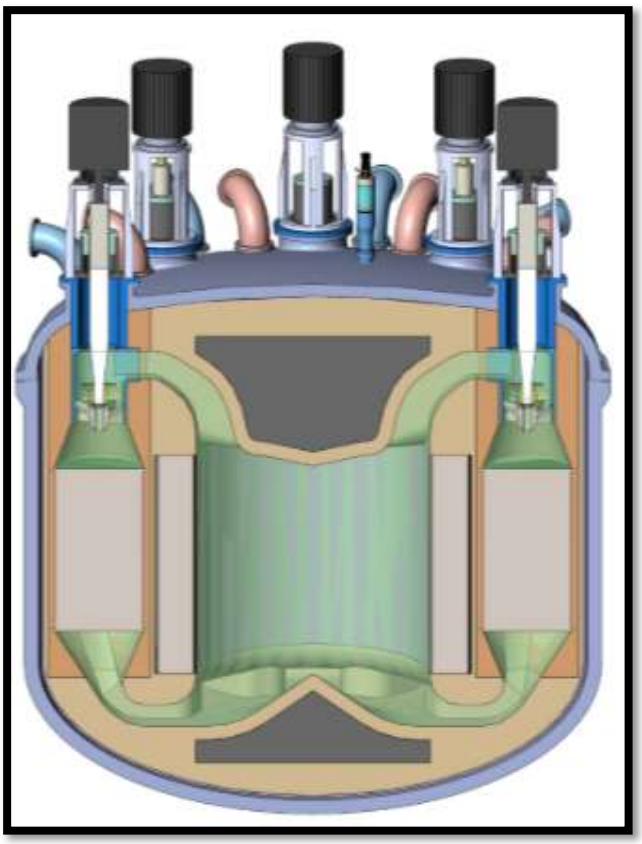

Figure 9. A diagram showing the conceptual design of the TerraPower molten chloride reactor experiment (TerraPower, 2020).[22]

In Canada, a company called Terrestrial Energy has developed the idea of an integral thermal molten salt reactor (IMSR). Terrestrial Energy is attempting to license a reactor that will integrate major plant components into one vessel. Figure 10 shown below is a visualization of the IMSR, along with proposed services it could aid. Due to the molten salt's enhanced thermal mechanics, the reactor will reach thermal efficiency upwards of 47% with a total power generation of 417 MW_{th}.[23] The IMSR is expected to

require an enrichment similar to existing LWR's and have a seven-year lifespan. The limited lifespan is due to the damaging behavior experienced by the graphite moderator in the IMSR core.[23]

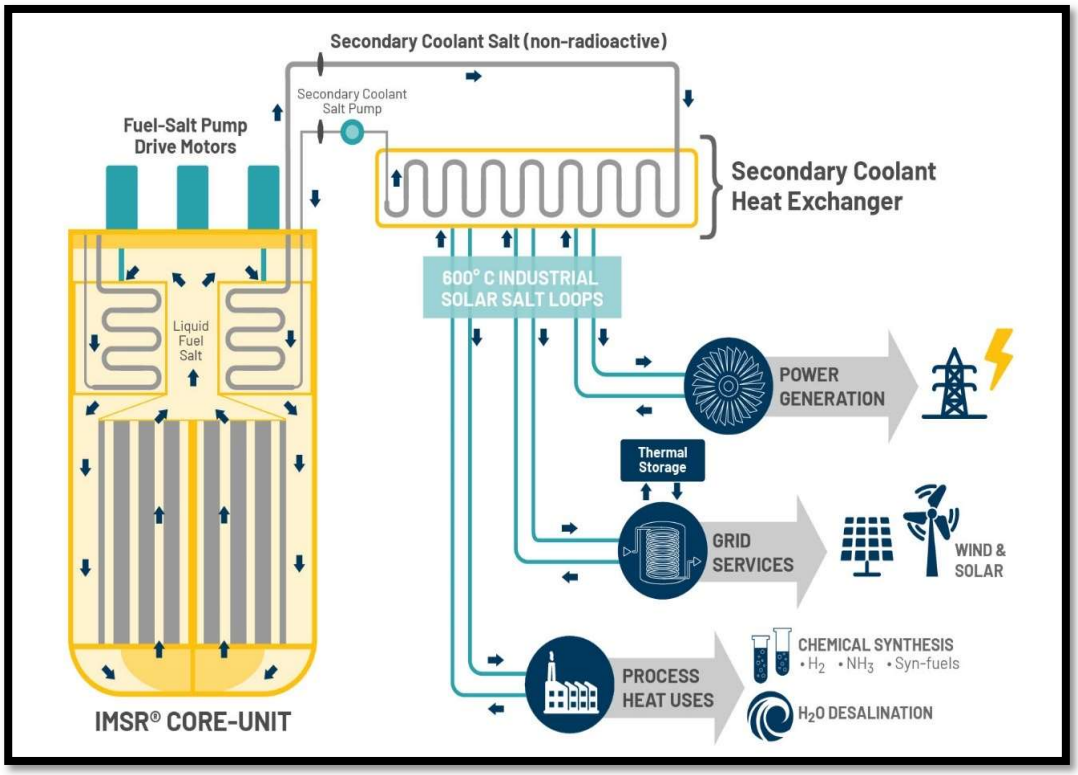

Figure 10. Visualization of the IMSR with proposed power and heat applications (Choe, 2018).[24]

In the Netherlands, a project named the Safety Assessment of the Molten Salt Fast Reactor (SAMOFAR) is underway. SAMOFAR uses experimental and advanced numerical techniques to prove the unique safety features of Molten Salt Fast Reactors (MSFR). The safety measures SAMOFAR is assessing include the freeze plug melting

and fuel salt draining, neutronics cross-section validation, coatings of structural material, the dynamic natural circulation of fuel salts, and the reductive process to extract lanthanides and actinides.[25]

These are just a few examples of the many MSR research projects around the world. Thus, this field of study within the nuclear engineering discipline is rapidly expanding and is soon to be at the forefront of clean energy production.

3. METHODOLOGY

3.1. Approach using MCNP

Designing the ThESA core was an iterative and highly coupled approach between the nuclear and the mechanical engineering teams. In the process of this work, a general Computer-Aided Design (CAD) model was translated into an MCNP model using the generalized geometry tools available in the MCNP neutronics code. The neutron source is modeled as an isotropic source with specified energy probabilities per angle. The neutron source was modeled by using a particle emission distribution table with the relevant energy histogram provided by experimental data from the Deuteron-Deuteron (DD) neutron generator manufacture Starfire Industries. Volume Flux (track length) calculations quantified the neutron flux and the reaction rates at the assembly's strategic points. The flux calculations were normalized with the appropriate magnitude for the neutron emission rate from the neutron generator. Appropriate variance reduction methods were incorporated in the MCNP input file to converge the simulation results statistically. An example of a simple variance reduction method is using weight windows to optimize neutron importance in ThESA regions of interest.[26]

3.1.1. Neutron Source Definition

The neutron source generator, the nGen – 400 manufactured by Starfire Industries(Champaign, IL), shown in Figure 11, was chosen for ThESA because of the high neutron emission rate of 2E8 neutrons/sec from the neutron generator. The generator produced neutrons in the range of 2MeV to 3 MeV. The high energy neutrons

are higher than the range of the fission cross-section of thorium-232 and will produce fission reactions in the FLiBe-Th salt.

Figure 11. Visualization of the nGen - 400 portable neutron generator (NGEN, 2019).[27]

The neutron generator was modeled using the data from the manufacturer that is visualized in Figure 12. The company Starfire Industries provided the emission characteristics for the DD neutron generator.

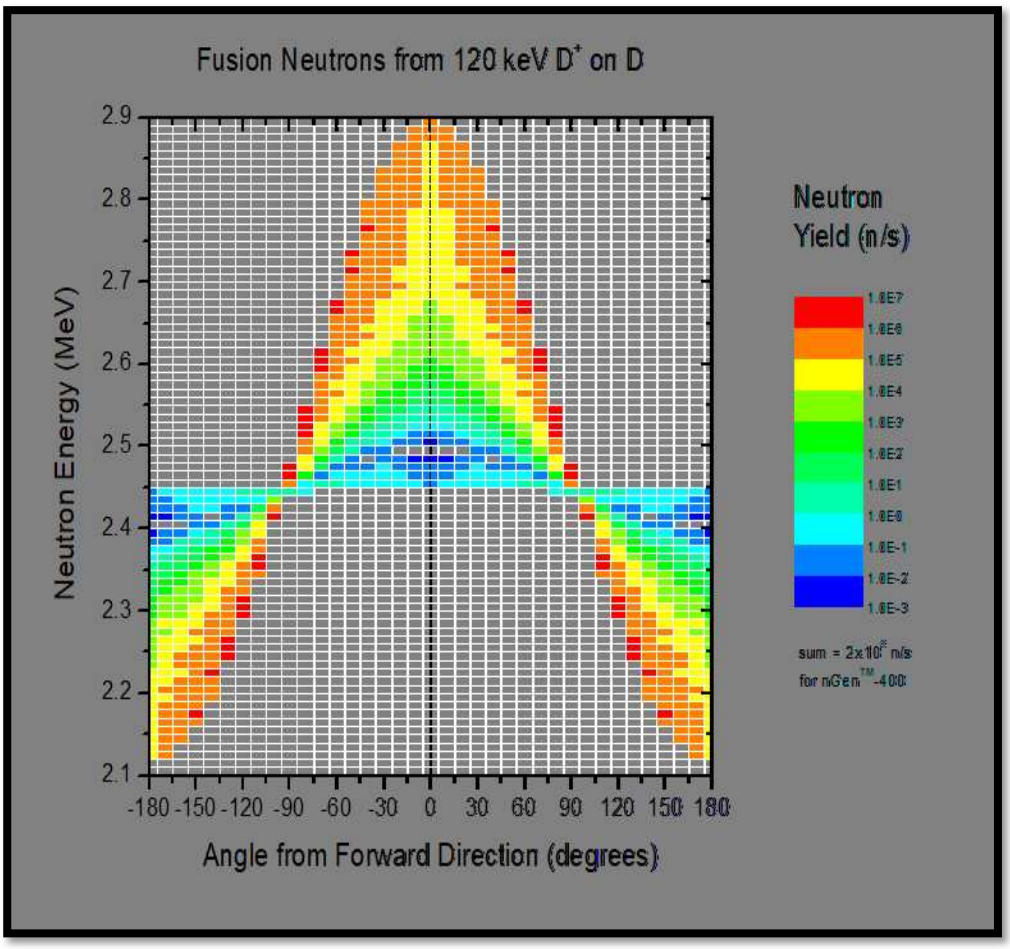

Figure 12. A histogram showing the angular distribution of neutrons (NGEN, 2019).[27]

The information provided by Starfire included the angle of emission and neutron energy range. The neutron yield (neutrons per second) was also given. Table 2 shows an example of some of the data provided by Starfire for the neutron distribution.

Table 2. A small sample data set provided by Starfire to calculate the distribution of neutrons.

Angle Min (deg)	Angle Max (deg)	Energy Min (MeV)	Energy Max (MeV)	Yield (neu/s)
0	5	2.42	2.43	0.0
0	5	2.43	2.44	0.0
0	5	2.44	2.45	0.0
0	5	2.45	2.46	0.076624
0	5	2.46	2.47	0.050163
0	5	2.47	2.48	0.023037
0	5	2.48	2.49	0.004029
0	5	2.49	2.5	0.0
0	5	2.5	2.51	0.005644
0	5	2.51	2.52	0.043798

The source definition was constructed by making neutron emissions within 19 possible angular bins in the cosine space. The direction linked neutron source information with 20 equally spaced values between cosine angular bins in the range of 1 (Cos 0°) and -1 (Cos 180°) with equal probabilities coded in the MCNP input file. The angular ranges provided by Starfire provided the number of bins. The energy distribution of neutrons provided by the Starfire was also coded in the MCNP input file. The probabilities of energies in each direction was based on the relevant neutron yield rates per energy. This configuration of the angular and energy distribution of neutrons from the generator towards the ThESA core should then accurately represent the neutron generator's behavior.

3.1.2. FLiBe-Th Salt Material

The materials team chose the LiF-BeF2-ThF4 (52.8-27.2-20 mol %) salt to be the primary FLiBe-Th salt used in the ThESA vessel. The FLiBe-Th mole fraction was recalculated per element in terms of mass fraction shown in Table 3. Appendix A lists all additional relevant material inputs that were used throughout the MCNP input files.

Table 3. The mass fractions representing the FLiBe-Th salt in MCNP and the atomic number mass identification (ZAID) numbers at 900K.

Element	ZAID	Mass Fraction
Li	3007.82c	0.041604
F	9019.82c	0.403741
Be	4009.82c	0.027828
Th	90232.82c	0.526828

4. NEUTRONIC CHARACTERIZATION BETWEEN PIN-TYPE AND POOL-TYPE ThESA CORE

4.1. Pin-type versus Pool-type Core Analysis of ThESA

ThESA aims to observe detectable quantities of neutrons born from fast fission of thorium-232 in the FLiBe salt medium. Thus, the design of ThESA aims to maximize the ratio of fission neutrons to external neutrons from the DD source. The maximization is to ensure that there are detectable levels of thorium fission neutrons. The effective neutron multiplication factor (k-eff) is an attribute of the system's geometrical and materials properties. Equation 1 shows the k-eff is dependent on the leakage of fast and thermal neutrons and material properties of the assembly. The k-inf represents only the materials properties while excluding the fast and thermal leakage factors. For the comparison study, only k-inf was calculated and considered to simplify reflector considerations.

$$\text{k-eff} = \eta\, f\, \rho\, \epsilon\, P_{FNL}\, P_{TNL}^{[28]} \qquad \text{Eq.(1)}$$

$$\text{k-inf} = \eta\, f\, \rho\, \epsilon \qquad \text{Eq.(2)}$$

Where:

- η The thermal Fission Factor, is the number of fissions neutrons produced per absorption in the fuel.
- p The resonance escape probability the fraction of fission neutrons that manage to slow down from fission to thermal energies without being absorbed.

ϵ The fast fission factor is the ratio of total fission neutrons to the fission neutrons from just thermal fissions.

f The thermal utilization factor is the probability that a neutron that gets absorbed does so in fuel material.

P_{FNL} The fast-non-leakage probability is that a fast neutron does not leak from the system

P_{TNL} The thermal non-leakage probability that a thermal neutron does not leak from the system

The assembly chosen in the comparison study should have the highest k-inf that is reasonably achievable. The highest k-inf is the assembly with the highest conversion of source neutrons into fission neutrons. Additionally, the final assembly design shall also consider the practicality of fuel loading, fuel transport, and fuel safety. This study compared two distinct assembly types to ensure the most optimal outcome for ThESA objectives.

Specifically, assembly designs with a pin or pool type fuel geometry were evaluated. The pin-type fuel study involved testing two different pin sets with varying fuel types. The first pin set design included only FLiBe-Th. The second pin set incorporated ThO_2 pins around the assembly center. The peripheral of the assembly would be filled with FLiBe-Th pins. The first pin set filled with only FLiBe-Th pins is named the homogenous set. The pool-type design would be a large vessel containing only FLiBe-Th with no pins. Both assembly types contained a DD neutron generator emitting source neutrons into the assembly. The resulting neutron interactions would

then proceed to induce fission, thus providing additional neutrons to the system in a cascading manner.

The same study used pins for the comparison due to ease of transportation and containment of fuel pins. Additionally, there is a large degree of experience using pin-type filled fuel in the commercial and research reactors. The pin-type fuel design is typical in both commercial and research reactors. Designs are such that the pellet contains the fuel material and is stacked and surrounded with specialized cladding in a pin so that the radioactive material remains physically separated from the coolant. This physical separation serves two critical functions. The first is that the radioactive material is never in direct contact with the coolant. Separation ensures minimal radioactive contamination and reduces operator radiation exposure since the coolant usually travels away from the reactor into non-shielded areas. The second function of cladding ensures an easy method for fuel shuffling and removal. The fuel removal occurs after a prolonged period in operation or upon reaching a specified burnup.

The burnup is dependent on the concentration of parasitic neutron absorbers and fissile material remaining. A high concentration of poisons leads to negative reactivity reducing the peak neutron flux amplitude within the assembly. The use of fuel shuffling maximizes the operation time of the fuel assembly. The pin-type design seemed natural as it would allow for convenient transportation, handling, and ease of disposal or storage at the end of life. Additionally, if ThESA fuel composition has to be altered, removing and replacing pins could easily be carried out. A pin-type style assembly would also benefit from the insertion of high multiplicity fuel at its center, such as substituting the

FLiBe-Th with ThO_2. The higher multiplicity fuel would lead to a higher fission chain reaction throughout the rest of the FLiBe-Th fueled filled pins.

A pool-type core would be more beneficial in a geometric sense as it would provide high a higher capability to absorb neutrons by reducing the void of inter-pin space. A pool-type reactor would require an assembly apparatus with reduced complexity. The pool-type would allow fission gasses to be released into the empty void space above the pool, ensuring reactivity was not impacted. The pool would be easier to ensure that radioactive material could not be easily stolen, as removing material from the pool would require significant effort in removing the primary vessel head similar to the pin-type.

4.2. Homogenous and Heterogeneous Pin Set Comparison

For the pin study, two-pin set assemblies were constructed for comparison. The pin set with the superior neutronics results will be compared against the pool type. The homogenous pin-set containing only FLiBe-Th is shown in Figure 13. The heterogenous mixed pin set containing thorium dioxide at the core center and surrounded with FLiBe-Th pins is shown in Figure 13 as well.

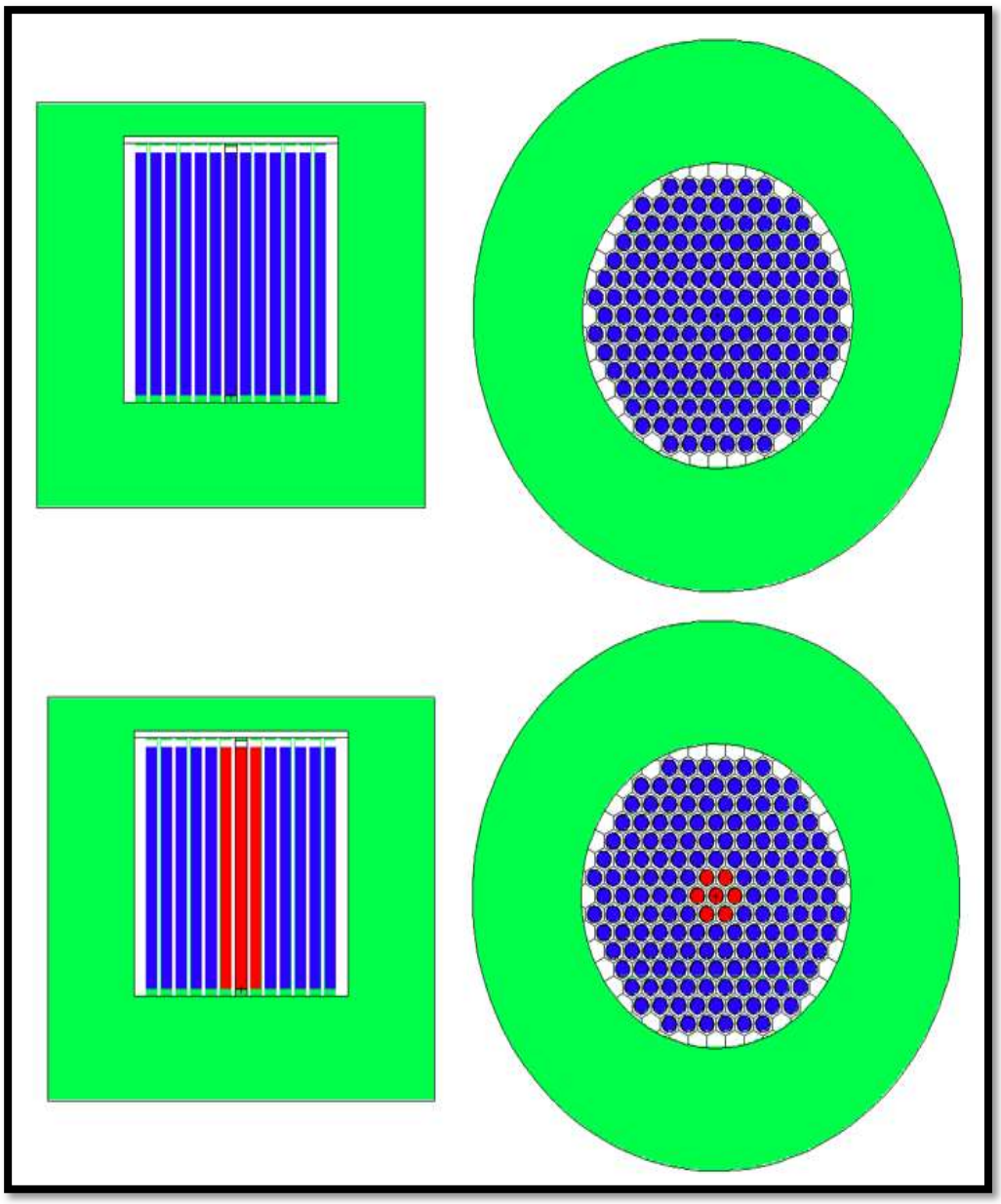

Figure 13. The two pins-types sets constructed with different fueled materials with the homogenous FLiBe-Th (top) and heterogenous thorium dioxide and FLiBe-Th (bottom).

4.2.1. Heterogeneous ThO_2 and FLiBe-Th Pin-Type Assembly Description

A heterogeneous pin-type assembly was constructed with a central pillar of pins that would contain ThO_2. Figure 14 is a visual representation of the geometrical model built within MCNP and visualized in the VISED software. The center pillar is fixed with ThO_2 due to a higher fission cross-section than the pure FLiBe-Th salt. The higher fission cross-section is due to the mass fraction of thorium to oxygen compared to the FLiBe-Th mixture. Outside the central pillar, FLiBe-Th salt fills the remaining pins shown in blue color in Figure 14. The ThO_2 pins would then produce neutrons primarily through fission and (n, Xn) reactions that would permeate throughout the core. The neutrons produced in the center would then lead to additional fission and other (n, Xn) reactions in FLiBe-Th salt pins. The pin walls were designed to be as thin as physically allowable. The pins would be composed of SS316L for maximum corrosion resistivity. The interior fuel pin cavity was 1.875 in or 4.7625 cm in diameter. The overall height for all pins was 36 in or 91.44 cm.

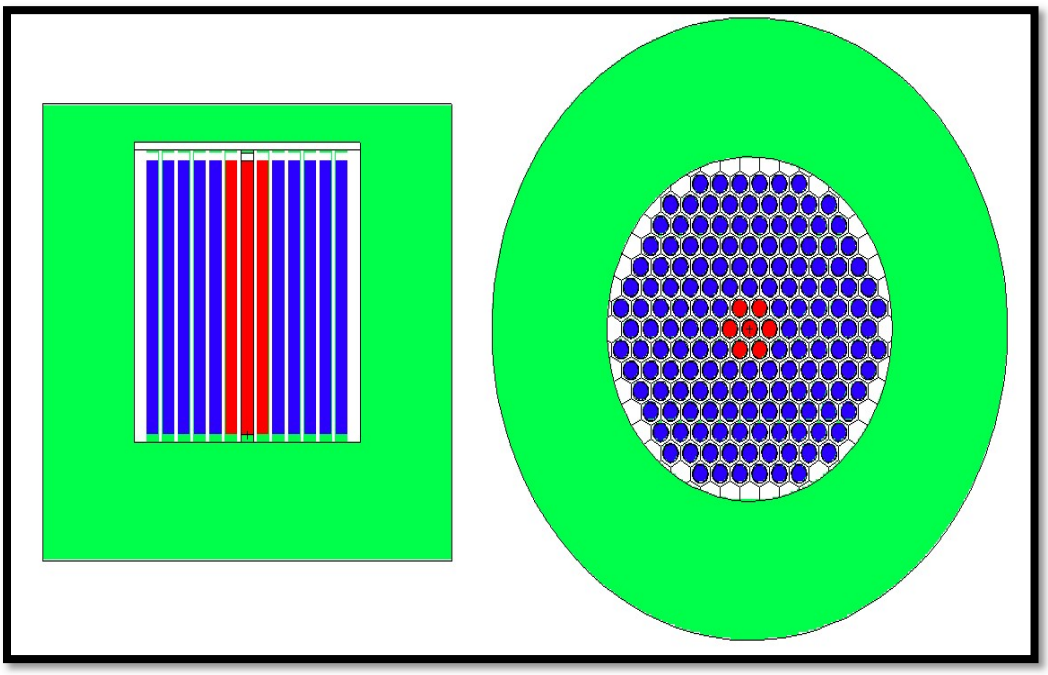

Figure 14. The mixed pin set with the center filled with thorium dioxide (red) surrounded by the FLiBe-Th salt pins (blue) encased in a vessel of standard stainless steel 316L.

4.2.2. Homogenous Pure FLiBe-Th Pin-type Assembly Description

The second design evaluated was identical to the previously mentioned heterogenous pin-type assembly. The only significant difference being the thorium dioxide in the center was replaced with pure FLiBe-Th. This procedure explored if the ThO_2 filled pins would yield an increased amount of fission neutrons. Theoretically, since this homogenous assembly contained less thorium-232 mass, it should produce

fewer fission neutrons than the mixed ThO_2 core. The dimensions for the height and interior fuel cavity remained identical.

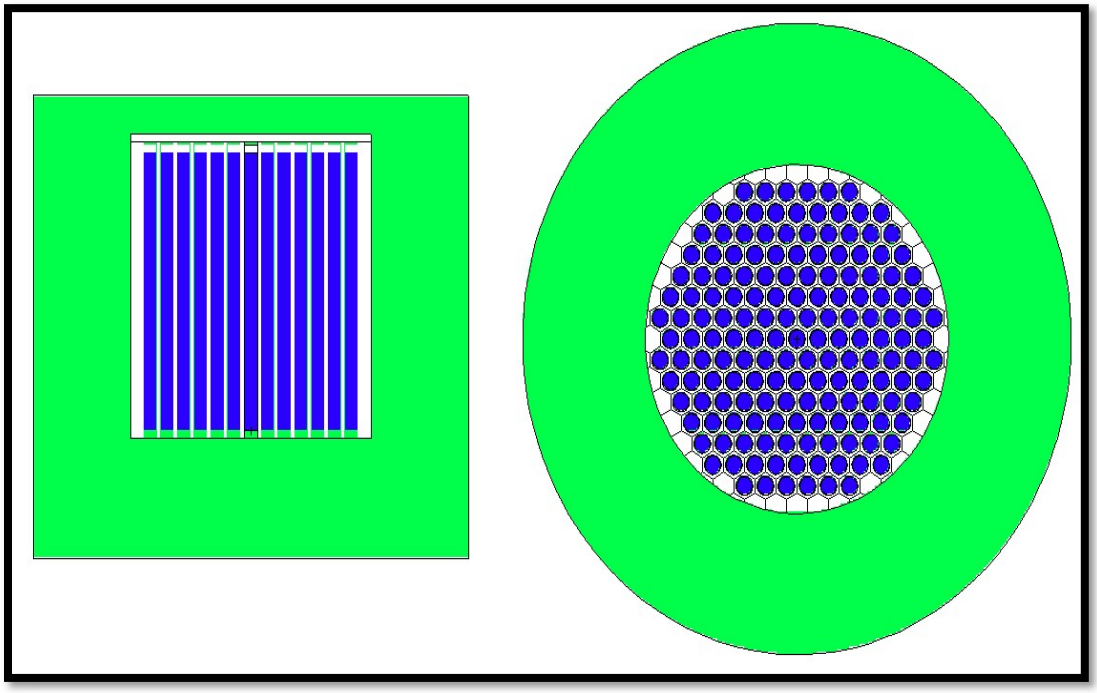

Figure 15. The pure pin set with the FLiBe-Th salt pins (blue) encased in a vessel of SS-316L.

4.2.3. MCNP Pin Assembly Construction

MCNP's hexagonal-grid array feature was used to construct a pin-type core input file with precise placement of unique fuel types at differing positions. The two different pin elements were created independently by using MCNP's universe-lattice feature. A cell containing the hexagonal array was created and used to develop both the mixed ThO_2 and the pure FLiBe-Th pin set. Figure 16 shows a snippet of the geometry cell section representing both fuel pin-types. For this study, the interior vessel's surface used the specular reflection boundary condition to compare only the assemblies' material characteristics. Thus, this specular reflection assured that the k-eff, calculated using the KCODE functionality of MCNP, was, in fact, k-inf.

```
Thorium Center (Increase Height and Axial increase Steel Reflector)
c Cell Cards
1 1 -3.788      -10 +12 -13              u=2 imp:n=1  $ Molten Thorium
2 0              -10 +13 -14             u=2 imp:n=1  $ Internal Fuel Cavit
3 2 -8.00       (+10:14:-12) -11         u=2 imp:n=1  $ Infinite Stainless
4 0              11                      u=2 imp:n=1  $ Exterior Steel Shel
c Thorium Oxide Pin
5 6 -10.000      -10 +12 -13             u=3 imp:n=1  $ Thorium Oxide
6 0              -10 +13 -14             u=3 imp:n=1  $ Internal Fuel Cavit
7 2 -8.00       (+10:14:-12) -11         u=3 imp:n=1  $ Infinite Stainless
8 0              11                      u=3 imp:n=1  $ Exterior Steel Shel
c Void Husk Hex outer most core
9 0 -100                                 u=1 imp:n=1  $ Void husk Hexagon
10 0 -24 25 -20 22 -23 21 lat=2 u=10       imp:n=1
     fill=-8:8 -8:8 0:0
     1 16R
     1 8R             2 2 2 2 2 2           1 1R
     1 6R           2 2 2 2 2 2 2 2 2       1
     1 5R          2 2 2 2 2 2 2 2 2 2      1
     1 4R         2 2 2 2 2 2 2 2 2 2 2     1
     1 3R        2 2 2 2 2 2 2 2 2 2 2 2    1
     1 2R       2 2 2 2 2 2 2 2 2 2 2 2 2   1
     1 1R     2 2 2 2 2 2 2 2 2 2 2 2 2 2   1
     1 1       2 2 2 2 2 2 2 2 2 2 2 2 2    1 1R
     1        2 2 2 2 2 2 2 2 2 2 2 2 2 2   1 1R
     1         2 2 2 2 2 2 2 2 2 2 2 2 2    1 2R
     1          2 2 2 2 2 2 2 2 2 2 2 2     1 3R
     1           2 2 2 2 2 2 2 2 2 2 2      1 4R
     1            2 2 2 2 2 2 2 2 2 2       1 5R
     1              2 2 2 2 2 2 2 2 2       1 6R
     1 1R             2 2 2 2 2 2           1 8R
     1 16R
11 0        -30 +31 -32 fill=10              imp:n=1 $MotherCell
12 2 -8.00   (30:-31:36) (-40 41 -37)       imp:n=1 $Steel Cage
13 0        (-30 32 -36)                   imp:n=1 $Vacumn
14 0        (40:-41:37)                    imp:n=0 $Death
```

Figure 16. The MCNP cell section snippet of inputs file used to construct the pool and differing variant pin-types.

4.3. Heterogeneous and Homogenous Pin-type Studies

4.3.1. k-eff studies for Heterogenous and Homogenous Pin-type Assembly

The key parameter to any nuclear system is k-eff. MCNP was used to solve for k-eff of each system independently. In this pin-type and pool-type study, a specular boundary condition simplified the leakage and reflector considerations. When tasked to find k-eff, MCNP solved for the k-inf factor because of the reflective boundary condition. This calculation does not consider the effects of leakage and thus solved for the effective neutron multiplication factor of an infinitely large system.

MCNP requires several inputs to calculate the k-inf. The KCODE feature of MNCP requires the number of neutrons used per cycle, an estimated guess of k-inf or k-eff, the number of neutron generation cycles to skip, and the total number of neutron generation cycles to simulate. Additionally, an initial fission site (KSRC) is also required. Typically, source points are placed within the fissionable material manually. However, the external neutron source definition generated the initial fission sites. Figure 17 shows the KCODE and KSRC inputs used in the MCNP input file. As per the best KCODE practices, 10,000 neutrons were used per cycle to ensure the proper statistical convergence of k-eff.[29] The value 0.1 served as the value guess because it needs to be close to the predicted calculated result. The number of cycles skipped, and the total cycles used in the MCNP input file were in accordance with KCODE simulation best practices.

```
c Data Cards SDEF [Block 3]
mode n
c mphys on
print 110 161 162
kcode 10000 0.1 50 500
SDEF  PAR=1 POS=0 0 96.52 VEC=0 0 -1 DIR=d55 ERG=FDIR=D56
```

Figure 17. MCNP KCODE input for both the homogenous and heterogenous assembly type.

Table 4 shows that the MCNP calculated values of k-inf for the homogenous and heterogenous pin cores calculated using the KCODE and KSRC inputs shown in Figure 13. These values would represent the effective neutron multiplication if the two systems were infinitely large. This process removes the complexities of reflector type and thickness in this comparison study. A parametric reflector was also performed, and the results of which are presented later in this thesis.

Table 4. The k-inf values calculated by MCNP with the specular boundary condition for the homogenous and heterogeneous assemblies.

Assembly Type	k-inf	k-inf standard deviation	Fuel Type
Heterogenous	0.02005	0.00002	ThO_2 & FLiBe-Th
Homogenous	0.01116	0.00001	FLiBe-Th

4.3.2. Flux studies for Heterogenous and Homogenous Pin-type Assembly

An F4 track-length flux tally feature of MCNP was used to calculate a cell average neutron flux within each pin fuel cavity, or per grid cell, to study the two pin-type assemblies. Since the fuel in the homogenous set contains only FLiBe-Th, this pin assembly only required a single repeated tally. The heterogenous pin set required two repeated tallies to ensure a separate ThO_2 measurement from the pins containing the FLiBe-Th. Figure 9 shows two flux profiles and amplitudes obtained for the homogenous and heterogenous pin-type assemblies.

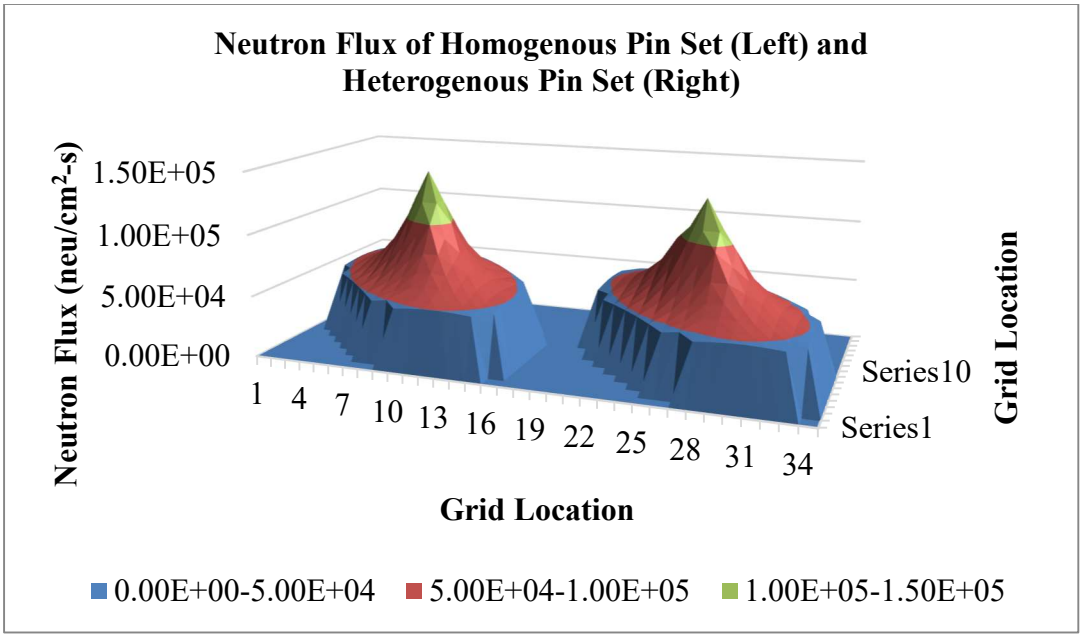

Figure 18. The neutron flux surface plots for the homogenous (left) and heterogeneous (right) pin-type ThESA assemblies.

Figure 19 depicts the relative error calculated by MCNP for the F4 flux tallies shown in Figure 18. The relative error increases by orders of magnitude as the flux propagates outwards into the assembly's peripheral. MCNP uses particle histories to calculate the F4 flux tally.[30] The amount of neutron simulation histories decides the relative error. Thus, since the center of the core has a higher particle history leads to a lower relative error in the center, and vice versa for the assembly's peripheral. F4 tallies require less than a 0.1 relative error to be considered accurate enough to be usable from a

statistical convergence perspective. The ten statistical tally checks required for the tally to be reputable also passed.

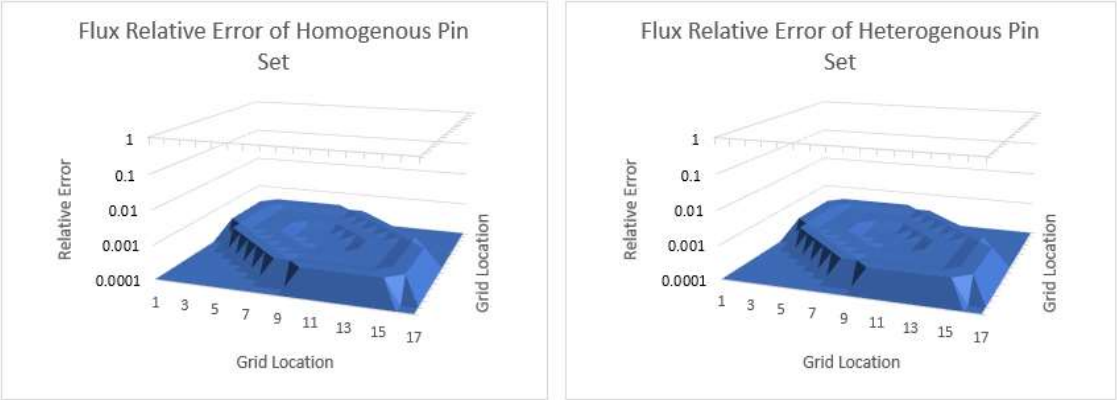

Figure 19. The relative error per grid cell for the homogenous mix (left) and the heterogenous pin set (right).

4.3.3. Fission Neutron Population for Heterogenous and Homogenous Pin-type Assembly

The neutrons that are born from fission are those that ThESA prioritizes. The pin set chosen must be one that would achieve a high neutron multiplicity and thus the pin set with the most critical configuration. An F4 tally was used in combination with a tally multiplier to calculate the assembly's average fission neutron population.

The tally multiplier used is the neutron source strength as a normalization factor for externally driven systems. An additional (-) operator, in conjunction with the normalization constant, directed MCNP to calculate the atom density in the designated tally volume.[31] Equation 3 shows the conversion to go from Fission Neutron Rate Density to Fission Rate. Equation 4 shows the different factors needed to calculate the fission rate density. The microscopic fission cross-section and the average number of neutrons produced per fission (ν) were used by calling the appropriate Evaluated Nuclear Data File (ENDF) number seen in Equation 4. Thus, using the repeat tally structure and a multiplier value, the fission neutron production rate was calculated per pin.

$$Fission\ Nuetron\ Rate\ Density = F4 * FM4 \quad \text{Eq.(3)}$$

$$F4 * FM4 = \Phi\ (-2E8)(\ 1)(-6)\ (-7) = \Phi\ \mathrm{N}\sigma_{\mathrm{f}}\nu_f \quad \text{Eq.(4)}$$

$$Neutron\ Rate = F4 * FM4 * Pin\ Volume \quad \text{Eq.(5)}$$

Where:

F4 The track length flux tally unnormalized (Φ).

FM4 The tally multiplier (flux normalization constant) (2E8).

-2E8 The neutron source strength (flux normalization constant) and a minus sign is used as an MCNP shortcut to calculate atom density (N) of chosen material within the volume being analyzed.

1 The material information from where cross-sections were drawn from, in this context, of ThO_2 and FLiBe-Th.

-6 The microscopic fission cross-section (σ_f).

-7 The average number of neutrons born per fission (ν_f).

Figure 20 shows a pair of surface plots for the fission neutron rate per grid cell. Figure 21 shows the resulting standard deviation for the fission neutron rate's surface plots per grid cell. The heterogeneous pin-type shows a sharper surface plot. This skew is due to the large difference between the center flux and the peripheral. The homogeneous pin set surface is far smoother because the difference in magnitude between the center and the core's peripheral was less pronounced.

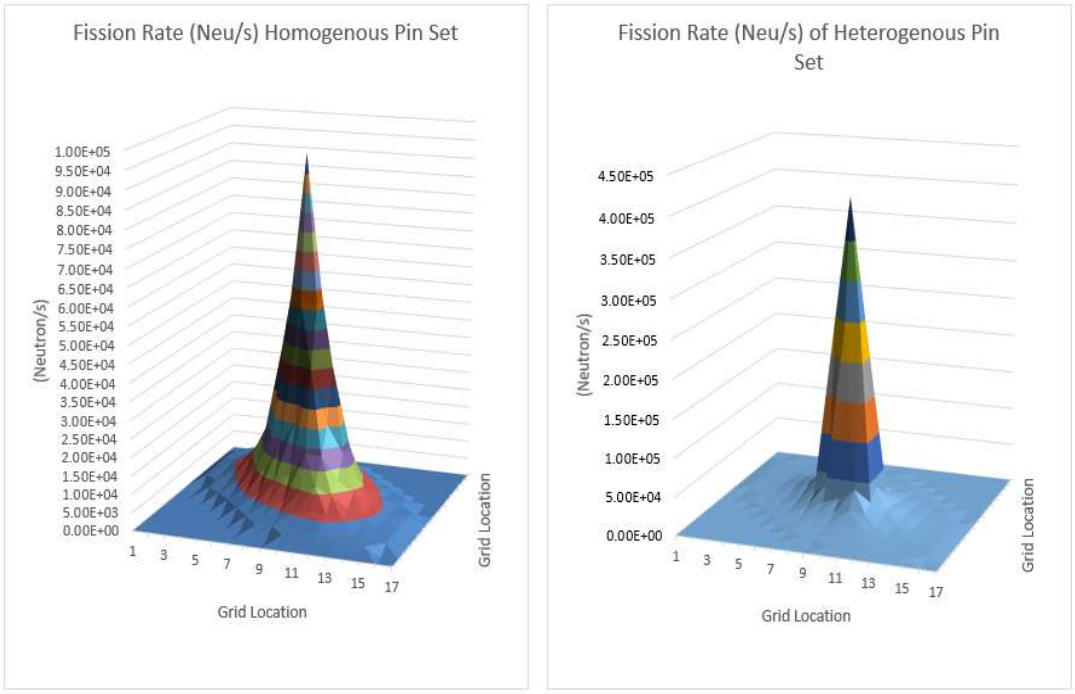

Figure 20. The fission neutron production per grid cell for the homogenous (left) and heterogeneous (right) pin sets.

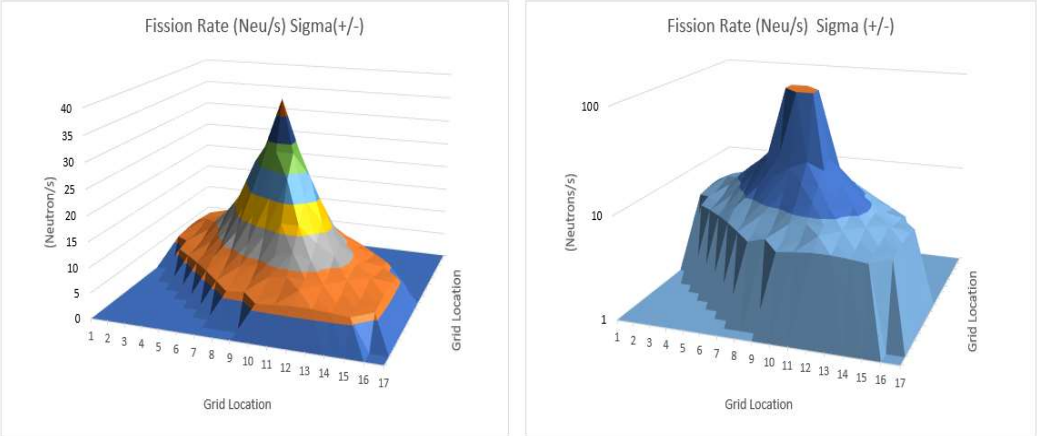

Figure 21. The standard deviation of the fission rate homogenous(left) and heterogonous(right).

4.3.4. Heterogeneous and Homogenous Pin Sets Results Comparison

Table 5 highlights the major difference between the different studies performed on the homogenous and heterogenous pin-type assemblies. The first significant study conducted was to ascertain the neutron flux shape and magnitude of both systems. It was expected that the heterogenous pin-type assembly would have a higher neutron flux than that of the homogenous. However, it did not have a higher peak neutron flux. The heterogenous ThO_2 pin-type assembly has a higher density by factor three compared to the FLiBe pins. Thus, the center thorium pins may have experienced a self-shielding effect from the source neutrons. Thus, with higher density, the neutrons could not permeate through the thorium dioxide fuel pins' entirety, leading to a lower peak neutron flux.

Table 5. A summary of the peak neutron flux and the average neutron flux between the homogenous and heterogenous pin sets.

Pin Set Type	**Flux Peak (n/cm^2-s)**	**Relative Error**	**Average Flux (n/cm^2-s)**	**Flux Sigma (n/cm^2-s)**
Homogenous	1.40E+05	0.0003	6.29E+04	1.99E+00
Heterogenous	1.32E+05	0.0003	6.12E+04	2.01E+00

Equation 6 is the reaction rate equation for neutrons produced from fission per second in a pin volume. Thus, if two systems have a similar neutron flux and volume but different macroscopic cross-sections, reaction rates would differ. Hence, additional studies were performed besides neutron flux to ascertain neutronic competitiveness.

$$Reaction\ Rate = \Phi\ \Sigma_f\ Pin\ Volume \qquad \text{Eq.(6)}$$

Where:

Φ The neutron flux (n/cm^2-s).

Σ_f The macroscopic fission cross-section of a fuel salt material (cm^{-1}).

$Pin\ Volume$ The volume within the pin filled with either thorium-dioxide or FLiBe-Th material (cm^3).

Table 6 highlights the fission neutron production rate differences between the homogenous and heterogenous pin-type assemblies. Although the peak and averaged fluxes are higher for the homogenous system, the total fission rate and average fission rate are almost higher by a factor of two for the heterogenous pin set. The larger total fission and average fission rate in the heterogenous pin assembly are due to the higher macroscopic cross-section of thorium-dioxide. The central pillar of thorium dioxide at the center, although suffering from self-shielding, is still compensated with a higher fission cross-section.

Table 6. The different fission rate densities between the homogenous and heterogenous pin core types.

Pin Set Type	**Fission Rate Peak (neu/s)**	**Sigma (neu/s)**	**Total Fission Rate (neu/s)**	**Sigma (neu/s)**	**Avg Fission Rate (neu/s)**
Homogenous	9.56E+04	5.07E+01	1.72E+06	158.21	1.10E+04
Heterogenous	4.05E+05	1.62E+02	3.16E+06	413.86	1.94E+04

The k-inf evaluation agreed with the results of the total fission rate calculation from Table. 6. The neutron reaction rate results indicated that the heterogeneous pin set had a higher neutron multiplicity than that of the homogeneous by a factor of two in the

total fission rate. Thus, the k-inf of the heterogenous pin set should also be higher by a factor of two. In Table 7, the k-inf values matched the results from Table 6.

Table 7. Effective neutron multiplication factor of homogenous and heterogenous pin-type assemblies.

Pin Set Type	k-inf	Relative Error of k-inf
Homogenous	0.01116	0.00001
Heterogenous	0.02005	0.00002

Thus, after evaluating the k-inf, the total fission rate, and the flux, the heterogenous pin set was the superior pin design. The heterogenous pin set is the configuration that will be compared to the pool-type to evaluate which performed superior from a neutronics perspective.

4.4. Pool-Type Studies

The secondary ThESA type tested and analyzed was the pool-type. The pool-type assembly would have a higher volume of fuel than the pin-type design. Thus, theoretically, it should have a higher effective neutron multiplication due to the increase

of thorium fuel. The mechanical team provided the physical limitations to the pool size. The pool size would be limited to a diameter no more than 36 in (91.44 cm) and a height of 18 in (45.72 cm). Figure 22 shows the graphical representation of the pool-type core and the ceramic heater, and the SS316L vessel encasing the core. This analysis used the specular boundary condition, similar to the pin-type ThESA, to simplify the comparison study between the pool-type and pin-type assembly. The reflective boundary condition was placed on the fuel cavity's interior like the pin-type ThESA study.

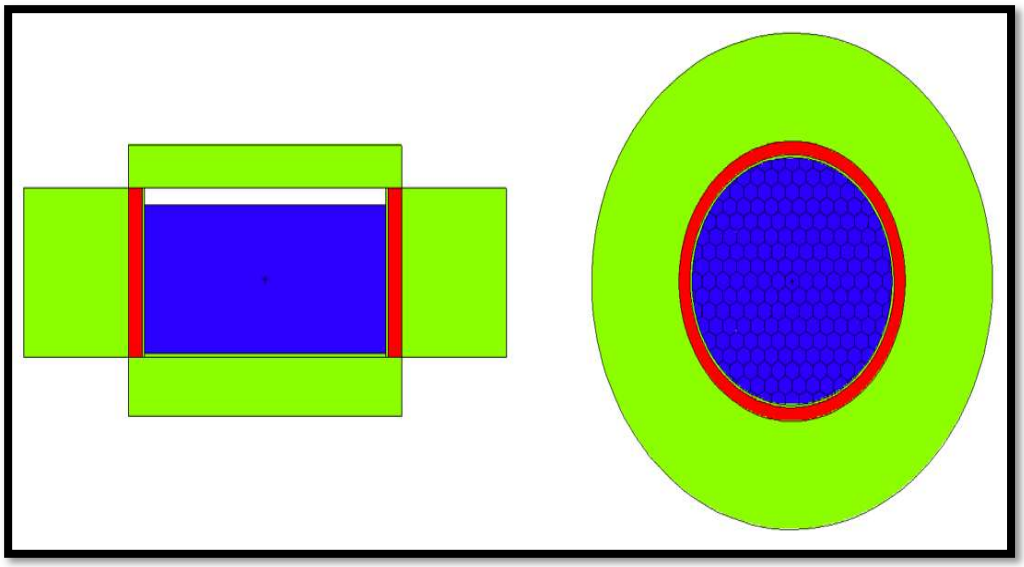

Figure 22. The pool-type core is filled with homogenous FLiBe-Th molten salt (blue) surrounded by a heater (red) and specular boundary condition.

4.4.1. MCNP Pool-type ThESA Construction

A snippet of the pool-type ThESA MCNP input file is shown in Figure 22. The pool-type MCNP input file was prepared using the “universe” feature of MCNP, where it has 100 cm in diameter and taller than the core's physical dimensions. That universe was cookie-cut by the hexagonal lattice grid. The only other significant physical change was a large ceramic heater surrounding the interior steel vessel that incased the fuel vessel. However, this would not affect the neutron multiplicity as the reflective boundary condition would ensure this material was never in contact with any neutrons for the comparison study.

```
Pool Type Core with Ceramic Heater and Reflector
c ccccccccccccccccccccccccccccccccccccccccccccccccccccccccccccc
c cell cards
1 1 -3.788 -14  1 -7  u=2 imp:n=1 $Thorium Fill Cylinder
2 0        -14  1 -7  u=9 imp:n=1 $Peri Zero
3 0 -24 25 -20 22 -23 21 lat=2 u=3        imp:n=1
     fill=-8:8 -8:8 0:0
     2 16R
     2 8R              2 2 2 2 2 2            2 1R
     2 6R           2 2 2 2 2 2 2 2 2         2
     2 5R          2 2 2 2 2 2 2 2 2 2        2
     2 4R         2 2 2 2 2 2 2 2 2 2 2       2
     2 3R        2 2 2 2 2 2 2 2 2 2 2 2      2
     2 2R       2 2 2 2 2 2 2 2 2 2 2 2 2     2
     2 1R      2 2 2 2 2 2 2 2 2 2 2 2 2 2    2
     2 2        2 2 2 2 2 2 2 2 2 2 2 2 2   . 2 1R
     2         2 2 2 2 2 2 2 2 2 2 2 2 2 2    2 1R
     2          2 2 2 2 2 2 2 2 2 2 2 2 2     2 2R
     2           2 2 2 2 2 2 2 2 2 2 2 2      2 3R
     2            2 2 2 2 2 2 2 2 2 2 2       2 4R
     2             2 2 2 2 2 2 2 2 2 2        2 5R
     2              2 2 2 2 2 2 2 2 2         2 6R
     2 1R              2 2 2 2 2 2            2 8R
     2 16R
4 0 -10 4 -5   fill=3 imp:n=1 $ Pool Mother
5 2 -7.92 10 -11 3 -6 imp:n=1 $ 304 SS Tub
6 3 -0.28 11 -12 3 -6 imp:n=1 $ Ceramic Heater
7 2 -7.92 12 -13 3 -6 imp:n=1 $ 304 SS Refl
c Axial Cell Cards
8  0        -10 5 -6          imp:n=1 $ Vacumn Atm Pool
9  2 -7.92  -10 3 -4          imp:n=1 $ SS Axi Tub Bot
10 2 -7.92  -12 1 -3          imp:n=1 $ SS Axi -Refl
11 2 -7.92  -12 6 -7          imp:n=1 $ SS Axi +Refl
c Neutron Death
12 0 (13:-3:6)(12:7:-1) imp:n=0  $ Neu Death
```

Figure 23. The geometry cell definition used to create the pool-type similar to the pin-type assembly.

4.4.2. k-inf Studies for Pool-type Assembly

The k-inf for the pool type filled with FLiBe-Th assembly was calculated to be 0.01288 +/- 0.00001. The value was calculated using the same parameters used for the pin variant study in line with the best KCODE practices.

4.4.3. Flux Studies for Pool-type Assembly

The researcher performed flux studies similar to that of the pin-type ThESA. The pool-type was compartmentalized into several hexagonal prism cells and filled with FLiBe molten salt. A neutron cell average neutron flux (F4 track length tally) was estimated in each cell and normalized with the neutron source generator. Figure 24 shows the flux distribution within the FLiBe-Th pool.

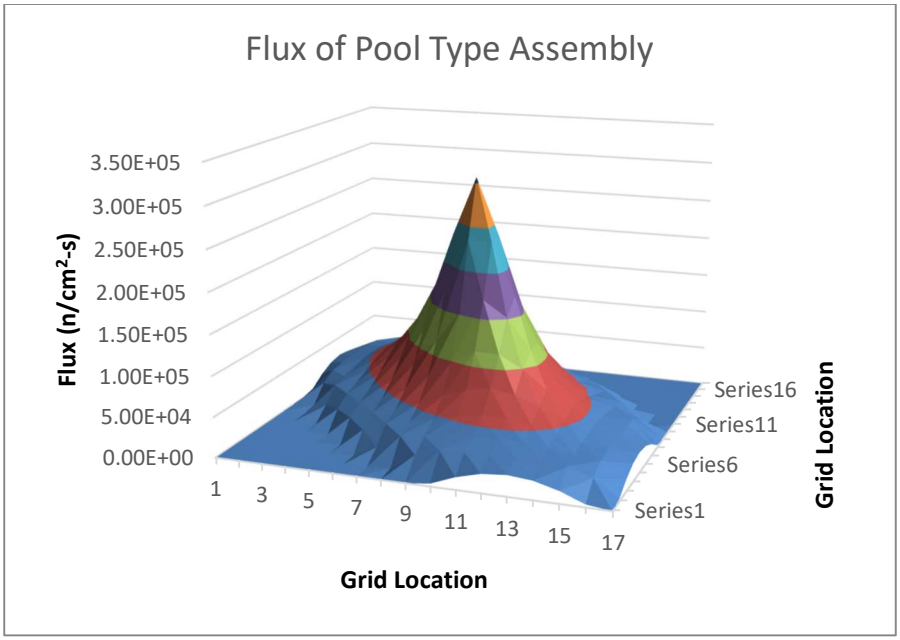

Figure 24. A surface plot of the neutron flux in the FLiBe-Th pool as a function of grid cell location.

The F4 tallies collected all had relative errors less than 0.10, passing all statistical checks by MCNP. Figure 25 shows the relative error for all tallies collected. As expected, the relative error increases toward the peripheral of the core. The increase is due to the neutron concentration as the track length tally depends on the number of neutron histories within its assigned volume.

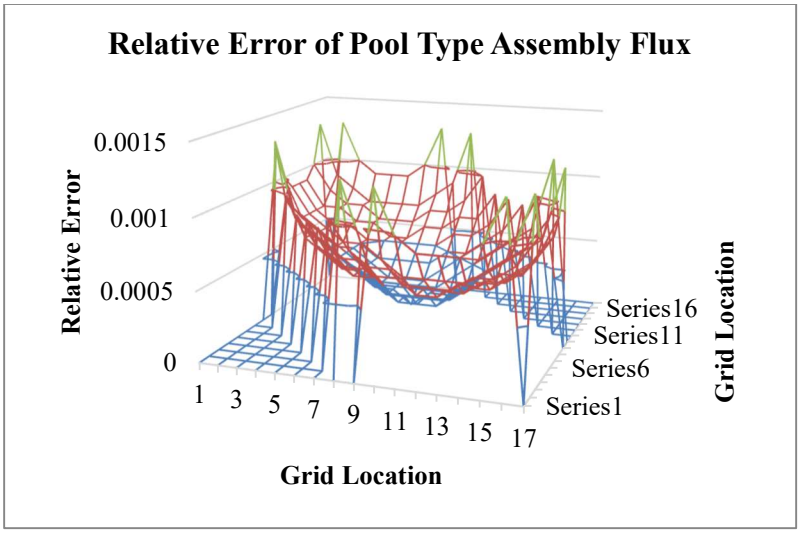

Figure 25. A surface plot of the relative error for each tally collected in the FLiBe-Th pool assembly.

4.4.4. Fission Neutron Population for Pool Type Assembly

The calculation for the fission neutron rate was identical to that of the pin-type. The neutron flux values were estimated per hexagonal cell grid and using neutron reaction rate multipliers shown in Equation 4, and it was converted to fission neutron rate density. Figure 26 shows the resulting surface plot of the neutrons produced per sec calculated per hexagonal prism cell in the pool-type ThESA.

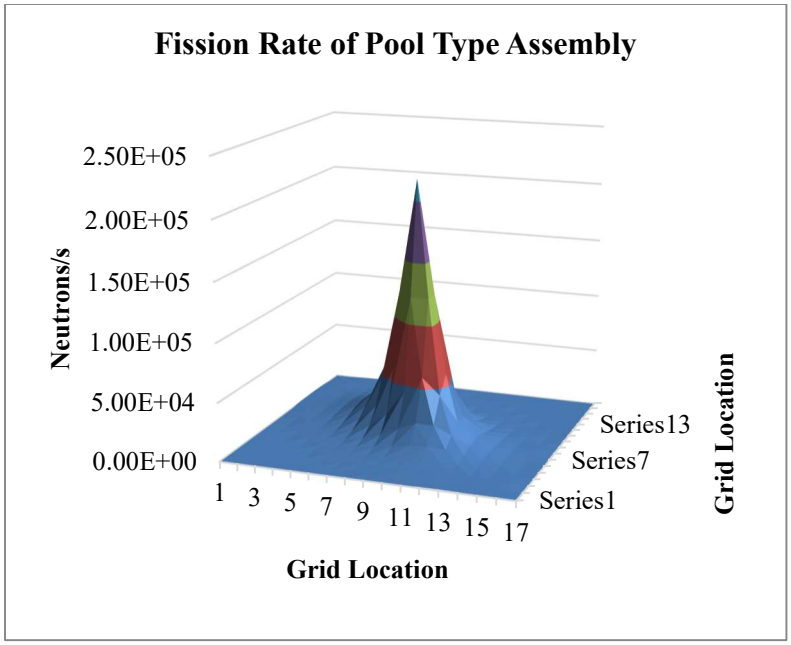

Figure 26. A surface plot of the neutrons produced per sec per grid cell location.

Figure 27 shows the standard deviation in the neutrons production rate from fission per grid cell location in a wireframe plot—a wireframe plot best represented the chart due to the peak at the assembly peripheral obstructing the center. The peaks in the pool surface fission rate are far sharper due to the decrease in neutron penetration throughout the pool from the Monte-Carlo simulation. Although the relative error at the peaks is far sharper than those in the pin configuration, all neutron fission flux tallies had relative errors less than 0.10, as seen in Figure 27.

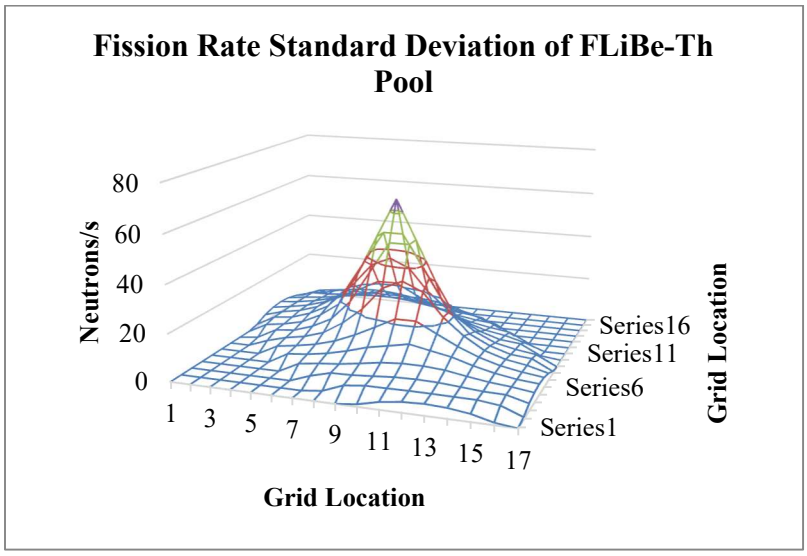

Figure 27. A wireframe surface plot of the fission rate sigma per grid cell location

4.4.5. Pool Assembly Results

Tables 8, 9, 10 are the cumulative study results calculated on the k-eff, neutron fluxes, and fission rate density for the pool-type ThESA. The results gathered are consistent with those used on the pin-type ThESA. The researcher normalized the results in a manner consistent with that of the pin-type as well. The only difference was in the volume used as the hexagonal prism was filled with FLiBe-Th instead of the volume of the interior fuel cavity of a pin.

Table 8. The neutron flux values for the pool-type assembly.

Peak Flux ($n/cm^2/s$)	Standard Deviation ($n/cm^2/s$)	Averaged Flux ($n/cm^2/s$)	Standard Deviation ($n/cm^2/s$)
3.07E+05	6.14E+01	5.93E+04	4.67E+02

Table 9. The fission neutron rate values for the pool-type assembly.

Fission Rate Peak (neu/s)	Standard Deviation (neu/s)	Total Fission Rate (neu/s)	Standard Deviation (neu/s)	Average Fission Rate (neu/s)	Standard Deviation (neu/s)
2.19E+05	6.56E+01	2.50E+06	2.21E+02	1.19E+04	1.05E+00

Table 10. The neutron multiplication factor for the pool-type assembly.

k-inf	k-inf std.
0.01288	0.00001

4.5. Comparison of Pin and Pool Results

Table 11 shows that the pool had a higher peak neutron flux at its center than in the pins. This can be explained by the smaller cross-sectional area of the pin fuel cross-section than the hexagonal prism cell containing the molten salt volume. The resulting interstitial space in the pin-type assemblies would result in a smaller effective solid angle. The resulting decrease in solid angle would then decrease the total peak neutron flux at the assembly center.

Table 11. The average and peak neutron flux difference between the heterogeneous pin-type and pool-type set up of ThESA with the specular boundary condition.

Assembly Type	**Flux Peak (neu/s)**	**Relative Error**	**Average Flux (neu/cm^2/s)**	**Standard Deviation (n/cm^2/s)**
Heterogenous Pin Set	1.32E+05	0.0003	6.12E+04	2.01E+00
Pool	3.07E+05	0.0002	5.93E+04	2.87E+00

Figure 28 shows that a larger portion of the heterogenous pins contained a higher neutron flux than that of the pool. This may be due to the neutrons' ability to permeate through the molten salt towards the core's top and peripheral reducing the overall particle history in the F4 tally volume.

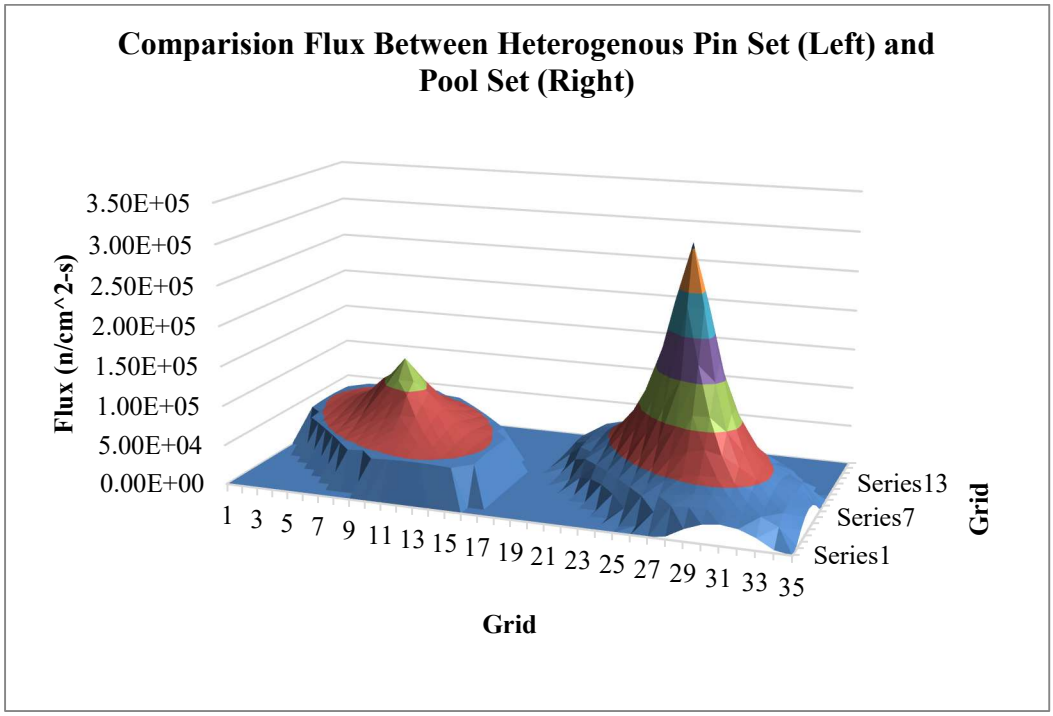

Figure 28. A comparison neutron flux chart comparing the distribution between the heterogenous pin-type (left) and homogenous pool-type configuration (right).

With comparable flux results, choosing one design over the other would have to combine operational limitations, a total number of neutrons produced in the peak flux-region, average fission rate throughout, and total fission rate.

The heterogenous pin set's peak fission rate was higher by a factor of three compared to the pool-type. The fission rate in the heterogenous pin type was higher even though the peak flux at its center was lower than the pool type. This difference is due to the ThO_2 pins having a higher fission cross-section because of the higher concentration of thorium than the FLiBe-Th salt.

The advantage of a higher fission cross-section, including a high quantity of fission neutrons at its center, caused an increase in the average neutrons and total neutrons produced throughout the heterogenous pin set core. Thus, the heterogenous pins outproduced the pool in the total fission rate shown in Table 12.

Table 12. The difference in fission neutron reaction rates between the heterogenous pin set and pool-type with specular boundary conditions.

Assembly Type	**Fission Rate Peak (neu/s)**	**Standard Deviation (neu/s)**	**Total Fission Rate (neu/s)**	**Standard Deviation (neu/s)**	**Avg Fission Rate (neu/s)**	**Standard Deviation (neu/s)**
Hetero	4.05E+05	1.62E+02	3.16E+06	3.28E+02	1.94E+04	2.53E+00
Pool	2.19E+05	6.56E+01	2.50E+06	4.14E+02	1.19E+04	1.05E+00

Although the heterogenous pin-type assembly had lower flux parameters, it was a superior choice in terms of total neutrons produced overall and at its center due to the

higher fission cross-section of ThO_2 compared to FLiBe-Th. However, the final design choice was also dependent on operational limitations. At the end of this comparison study, 36 in pins were not physically capable of fitting in the glovebox for FLiBe-Th salt production during the design process. Thus, it was recommended by the mechanical engineering team to adopt a maximum limit of 18 in to any conceptual comparison study. Therefore, there was consideration towards double stacking 18 in pins to mimic the original 36 in design. An example of double-stacked pins is shown in Figure 29. However, the mechanical team's further analysis revealed complexities in filling the pins as the salt would need to be melted in the lab to fill the pins. After transporting, the pins would need to be re-melted after being situated in the primary vessel. Onsite melting of all the pins would have been an arduous and complicated task.

Additionally, adding a welding capability within the manufacturing glovebox to seal the pins was considered but rejected as custom complex modifications would have been necessary. Thus, since the 36 in pins were only marginally superior, the decision was made to proceed with the pool style as it was easier to manage from an operational perspective. The design going forward would include heaters, firebricks, vacuum spaces, and a parametric study to ensure neutron reflection would be necessary and justifiable within the project goals.

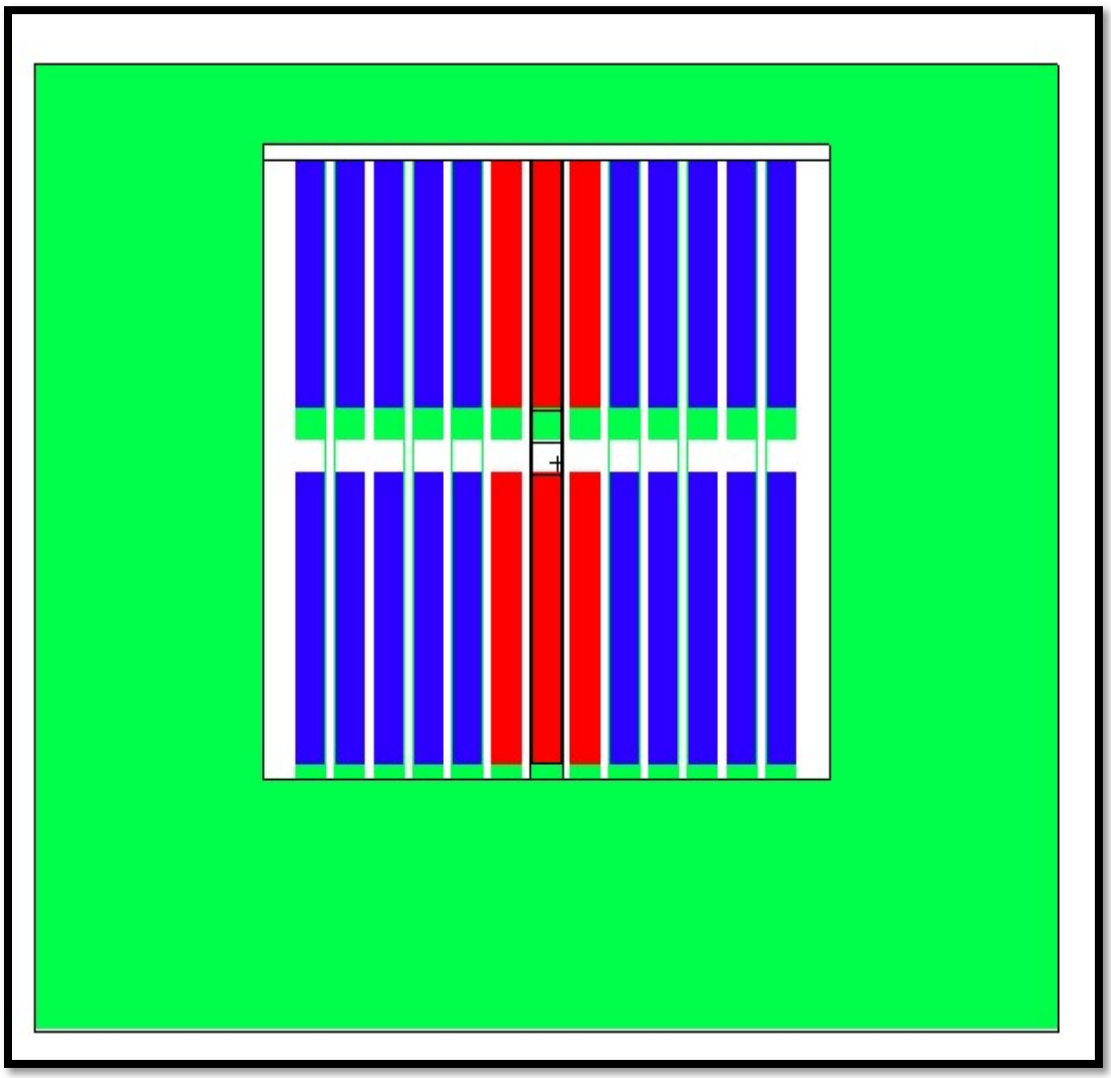

Figure 29. The proposed double-stacked heterogenous 36-inch pin set with ThO_2 (red) and FLiBe-Th (blue).

5. PARAMETRIC STUDY ON REFLECTION BOUNDARY OF THESA

5.1. Reflection Boundary Condition at the Assembly Periphery

The previous section determined the type of assembly that the ThESA project would use to proceed. The next natural step of the analysis was to determine if a reflector would be necessary after removing the pool-type assembly's specular boundary condition. The previously observed specular boundary condition helped simplify the comparison study between the pool and pin-type assemblies. ThESA primary objective is to maximize the neutrons produced from thorium-232 fissioning. Thus, a parametric reflector study would analyze the neutronics benefits added to the assembly.

A reflector is typically used in most reactors to minimize the neutron losses and reduce the total critical mass to achieve a specific value for k-eff. In ThESA case, a reflector was considered to increase the k-eff of the system. An increase in k-eff would help ThESA maximize the number of neutrons produced from thorium-232 fissioning. Table 13. shows the difference in total neutrons produced from fission by using the specular boundary condition. This condition proceeding forward would be inactive so that all calculations moving forward would account for neutron leakage in the system.

Table 13. A comparison showing the effect of the specular boundary condition used in the pin pool comparison study.

	Specular Boundary Condition	k-eff	Total Neutron Rate (neu/s)	Percent Difference
Pool	Active	0.01288	2.500E+06	0%
Pool	Inactive	0.01201	2.42E+06	-3%

The reflector material chosen to study would need to be a high Z material compared to typical thermal reflectors such as graphite, water, and heavy water. A low-Z material would moderate the reflected neutrons increasing the rate of thermal thorium breeding into uranium-233. Figure 30 shows that thermal neutrons would induce absorption and lead to the production of uranium-233. Stainless Steel 304 (SS) was chosen because it would serve the dual purpose of a containment vessel and a fast neutron reflector. Other more exotic reflectors were considered, such as beryllium carbide, magnesium oxide, and zirconium silicide. However, none could serve the same dual purpose as SS304. Additional tests using zirconium silicide examined the neutronic difference between an exotic and standard reflector such as the SS304. More so, other consideration factors included manufacturing, accessibility, and cost of the reflector.

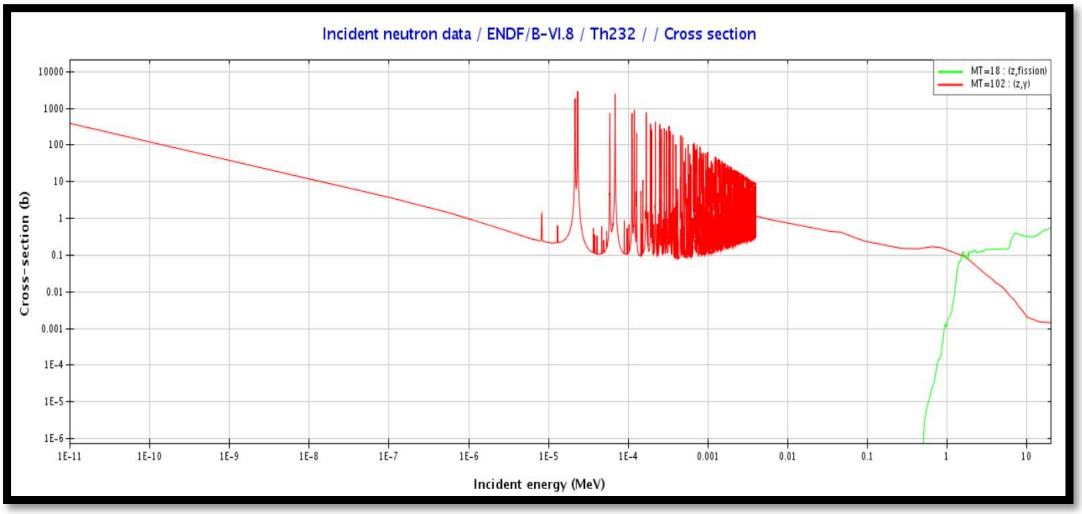

Figure 30. The thorium-232 fission and capture cross-section compared as a function of energy (Janis, 2020).[32]

5.1.1. Calculation of Inelastic Mean Free Path for Optimal Reflector Thickness

MCNP simulations of nuclear systems with large reflectors can be computationally expensive. Thus, two methods were employed to reduce the guess and check style using MCNP on optimal reflector depth. The first method suggested by Dr. Sunil Chirayath at Texas A&M University was that 3 Inelastic Mean Free Paths ($MFP_{Inelastic}$) should be the most optimal reflector thickness.[33]

The calculation of $MFP_{Inelastic}$ required using the Java-based Nuclear Data Information System (JANIS) and Evaluated Nuclear Data Library (ENDF/B-VIII). Equation 7 shows that the MFP is a straightforward calculation once the macroscopic

cross-section for an inelastic scattering ($\Sigma_{Inelastic}$) is known. The calculation of $\Sigma_{Inelastic}$ in Equation 8 is very intricate. The inelastic microscopic cross-section ($\sigma_{i-inelastic}$) of all constituent elements required calculating first, along with their respective atom densities (N_i) in the SS304. Equation 9 was used to calculate the N_i for all constituents elements in SS304. The $\sigma_{i-inelastic}$ of each constituent element in SS304 was calculated using Equation 10. which followed the ENDF sum rules for inelastic scattering.[34] The rules revealed the inelastic microscopic cross-section was the total sum of individual cross-sections that were inelastic reactions. This summation was performed for every constituent element in SS304 then multiplied by respective atom density. The summation performed in Equation 10 would then be equivalent to that of the SS304 inelastic scattering cross-section.

$$MFP_{Inelastic} = \frac{1}{\Sigma_{Inelastic}} \quad \text{Eq.(7)}$$

$$\Sigma_{Inelastic} = \sum_{i=elements\ in\ steel} N_i * \sigma_{i-inelastic} \quad \text{Eq.(8)}$$

$$N_i = ((\rho_{SS304} * W_i) * \frac{N_A}{MW_i}) \quad \text{Eq.(9)}$$

$$\sigma_{i-inelastic} = \sum_{j=4,5,11,16-18,22-37,41-42,44-45} \sigma_j \quad \text{Eq.(10)}$$

Where:

$MFP_{Inelastic}$ The average neutron path before an inelastic collision occurs (cm).

$\Sigma_{Inelastic}$ The macroscopic cross-section accounting for the constituent's elements in steel for inelastic scattering (cm^{-1}).

N_i The atom density per constituent steel component ith (atoms-cm^{-3}).

$\sigma_{i-inelastic}$ The microscopic cross-section of the ith steel constituent (cm^2).

W_i The weight fraction of the ith constituent in the SS304.

MW_i The molecular mass (g/mol).

ρ_{SS304} The density of stainless steel 304 (g/cm^3).

N_A Avogadro number (atoms/mole).

σ_j The microscopic cross-section that represents reaction dictated by ENDF to represent non-elastic reactions (cm^2). [34]

Table 14. shows all the individual constituent elements in SS304 and their respective weight percent, atom density, and macroscopic inelastic cross-section. The MFP for inelastic scattering calculated is 13.29 cm. Then 3 MFP meant a total SS304 reflector thickness of approximately 40 cm requirement top optimize neutron leakage from the ThESA pool.

Table 14. Individual weighted components of elements SS304 and the calculation of the inelastic scattering cross-section.

	Weight Percent (%)	**Molecular Weight MW (g/mol)**	**Atom Density (atoms/ b-cm) N_i**	**Sigma Inelastic $\sigma_{i-inelastic}$ (b)**	**Weighed Sigma inelastic $\Sigma_{i-inelastic}$ (b)**
Ni	8.000	58.69	6.59109E-03	1.43E+00	9.43E-03
Cr	17.500	52.00	1.62751E-02	6.82E-01	1.11E-02
Mo	0.000	95.96	0.00000E+00	1.34E+00	0.00E+00
Fe	71.270	55.85	6.17133E-02	8.51E-01	5.25E-02
Si	1.000	28.09	1.72177E-03	1.80E-01	3.09E-04
Mn	2.000	54.94	1.76041E-03	1.05E+00	1.85E-03
C	0.070	12.01	2.81829E-04	0.00E+00	0.00E+00
P	0.045	30.97	7.02546E-05	5.34E-01	3.75E-05
S	0.015	32.07	2.26212E-05	9.45E-02	2.14E-06
N	0.100	14.01	3.45239E-04	0.00E+00	0.00E+00
				$\Sigma_{Inelastic}$ (cm^{-1})	7.52242E-02
				$MFP_{Inelastic}$ (cm)	1.32936E+01

An alternative method used validated the optimal thickness calculated using the inelastic MFP. The maximum thickness that a reflector could be without additional benefits, according to diffusion theory, was two times the diffusion length (L) in the reflector.[35] This coefficient can be calculated as seen in Equation 11 by squaring the

division of the reflector's diffusion coefficient by the macroscopic absorption cross-section. The group constants were attained from a journal paper *Reactivity Effect of Iron Reflector in LWR Cores*.[36] Since SS304 has an iron weight composition of 71.27%, according to Table 15, it would serve as a close approximation to pure iron. The optimal reflector thickness (δ) calculated from Equation 12 was 41.97 cm.

$$L = \sqrt{\frac{D_{Reflec}}{\Sigma_{Abs-Reflec}}} \qquad \text{Eq.(11)}$$

$$\delta = 2\,L \qquad \text{Eq.(12)}$$

Where:

L The diffusion length is the mean square distance that a neutron travels in one direction from the plane source to its absorption point (20.988 cm).

D_{Reflec} The proportionality constant between the current density and gradient of neutron the neutron flux (1.144 cm).

δ The optimal reflector thickness (41.976 cm).

Table 15. The results of the two analytical methods to calculate optimal reflector thickness.

Method	Optimal Reflector Thickness (cm)
3 Inelastic MFP	39.88
2L Diffusion Length	41.97

5.1.2. Parametric Reflection Results

To effectively study whether a reflector would benefit ThESA, the following data was generated the k-eff, total neutrons produced from fission per second, and averaged neutron flux. The tallies resulted from using multiple MCNP files; simulations were carried out by varying reflector material and thickness. All inputs would have the specular boundary condition, previously used in the pin-pool comparison study, removed. The inelastic MFP was used as a parameter to vary on three separate reflector thicknesses. Both reflector thicknesses were adjusted for material type.

The criticality calculation used MCNP's KCODE functionality with varying inputs by differing reflector thickness in inelastic MFP terms. The KCODE feature, in conjunction with the source definition, identified the original fission sites. The average neutron flux was determined using an F4 tally placed over the entire pool assembly. The neutron source strength was used as the normalization constant with the FM multiplier feature of MCNP. The total neutrons produced per second resulted from the averaged neutron flux and the necessary cross-section reaction numbers, and the neutron source

strength and total pool volume. Table 16 shows the parametric reflection study results performed by varying the inelastic MFP and the reflection material type.

Table 16. The tally and kcode results as a function of both inelastic MFP and reflector material type.

Stainless Steel 304						
MFP (cm)	**k-eff**	**Relative Error**	**Total Neutron Population (neu/s)**	**Relative Error**	**Averaged Neutron Flux (n/cm^2/s)**	**Relative Error**
0*	0.01201	0.00001	2.424E+06	0.0001	4.90E+04	0.0001
1	0.01205	0.00002	2.441E+06	0.0001	5.31E+04	0.0001
2	0.01205	0.00001	2.441E+06	0.0001	5.35E+04	0.0001
3	0.01207	0.00002	2.441E+06	0.0001	5.35E+04	0.0001
Zirconium Silicide						
MFP (cm)	**k-eff**	**Relative Error**	**Total Neutron Population (neu/s)**	**Relative Error**	**Averaged Neutron Flux (n/cm^2/s)**	**Relative Error**
0*	0.01201	0.00001	2.424E+06	0.0001	4.90E+04	0.0001
1	0.01204	0.00002	2.439E+06	0.0001	5.20E+04	0.0001
2	0.01204	0.00002	2.440E+06	0.0001	5.25E+04	0.0001
3	0.01205	0.00001	2.440E+06	0.0001	5.26E+04	0.0001

**The parameter 0 MFP is just the MCNP input without the reflective boundary position with no reflector.*

5.1.3. Conclusion

The decision to include or exclude a reflector was also dependent upon factors other than neutronics benefits. The neutronic benefits would need to justify the cost and complexities added to the project. The reflector needed to be proved practical in the sense of manufacturability within project resources and timeline contexts. Since the goal of ThESA is to maximize thorium fission, the reflector should act to maximize the neutron population and add significant benefit to that goal. Figure 31. depicts the systems k-eff as an increasing function of reflector thickness by inelastic MFP length in SS304. The same reflector thickness was also used for the zirconium silicide reflector to compare the two cases per depth. Figure 31 shows that there is an increasing trend in k-eff as reflector thickness increases. The preferred reflector material is SS306 due to its superior reflection qualities, availability, and ease of local sourcing. The zirconium silicide does not appear to be a more effective reflector as a function of thickness compared to the SS306.

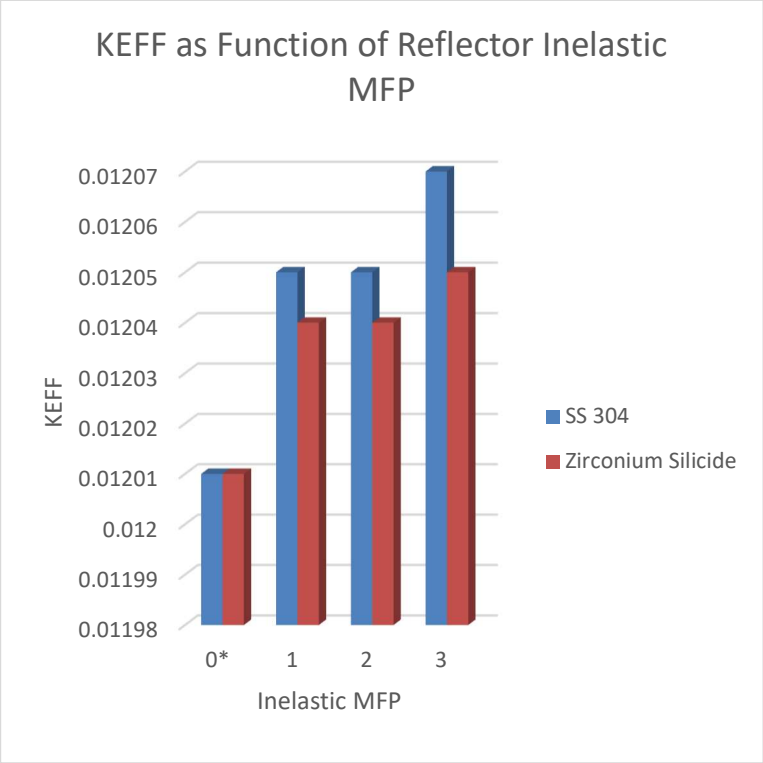

Figure 31. The k-eff of the system with increasing reflector thickness as a function inelastic MFP.

To definitively conclude, the total neutron production per second was used as the final metric to compare the relative effectiveness between no reflector, SS304, and zirconium silicide. Figure 32 shows an increasing trend as a function of increasing reflector thickness. The results predict that the SS304 reflector is a more effective neutron reflector in this particular case.

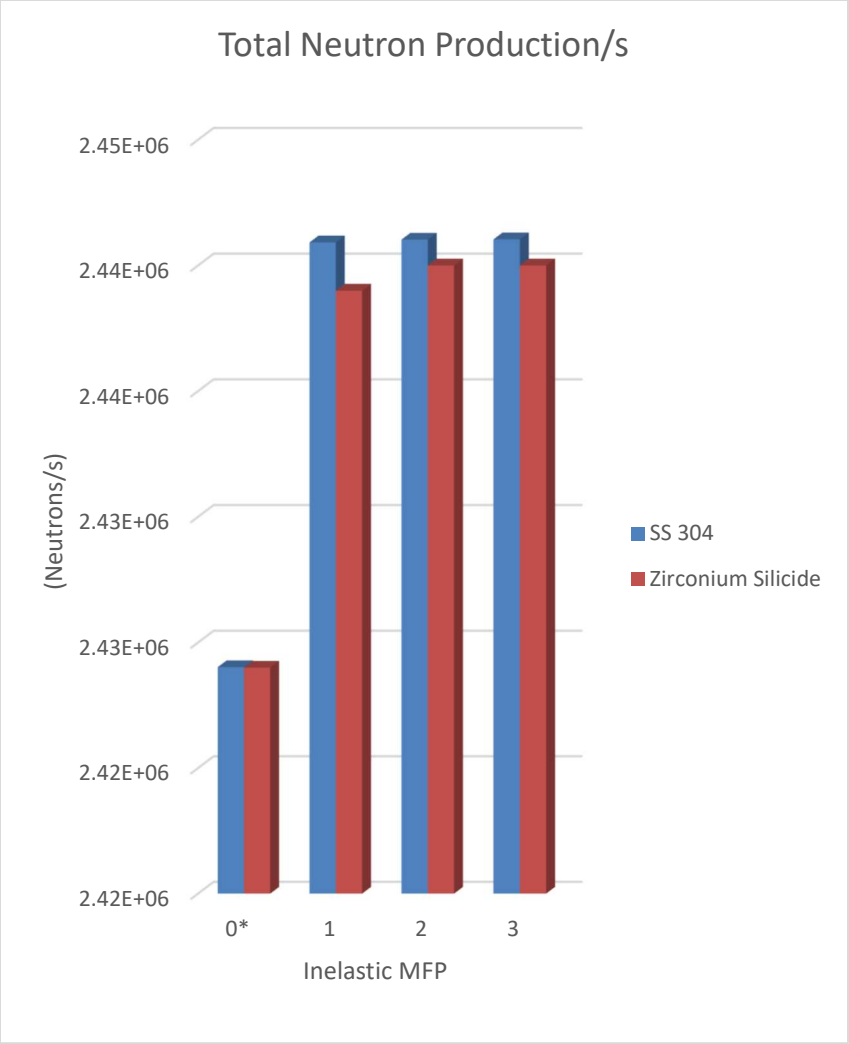

Figure 32. The total neutron production rate from fission per second increases reflector thickness in terms of inelastic MFP.

Figure 33 compares the reflector with associated uncertainty visually. Thus, Figure 33 shows that the two results between SS304 and zirconium silicide are

statistically different, and from a neutronics performance point of view, SS304 is a better choice.

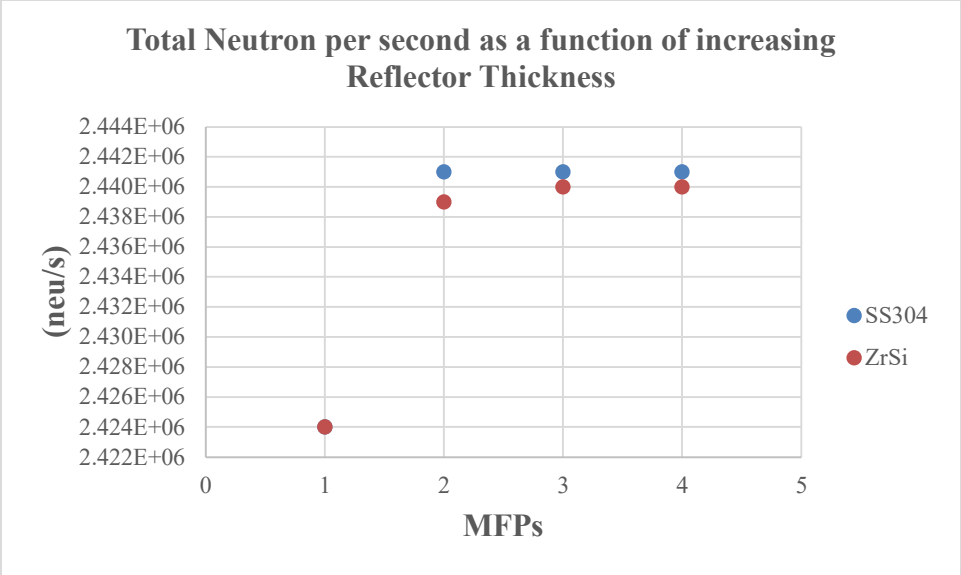

Figure 33. The total neutrons per second produced as a function of increasing reflector thickness in terms of inelastic MFP with uncertainty.

Table 17 predicts only a 1.0 % difference in total fission neutrons per sec between the most optimal neutron reflector and no reflector. The perfect reflector on the initial study was, in practice, the effective neutron multiplication factor of a system that is infinitely large with no neutron leakage. Thus, reflection results can never be equal to

the perfect reflector but aim to approach the k-inf value. Without reflection, the total fission neutron population experienced a 3% reduction. After analyzing different thicknesses, the most optimal value calculation occurred at the predicted 3 MFP or two diffusion lengths. The resulting neutron population reduced the total difference between the perfect reflector and the most optimal from a 3.0 % to 2.0 % difference.

Table 17. The pool's neutronics results with a perfect reflection boundary, no reflector, and the thickness reflector configuration.

	Reflective Boundary	**k-eff**	**Total Neutron/s Rate**	**Percent Difference**
Pool	Perfect Reflector	0.01288	2.500E+06	0%
Pool	None	0.01201	2.420E+06	-3%
Pool	SS304 3-MFP	0.01207	2.441E+06	-2%

With the most optimal reflector, the only increase neutron population observed was about 1% compared to the bare case; the reflector's cost should be considered to make a design decision to include it in the final design or not. According to Table 18, the raw material's cost to construct the optimal reflector would be approximately thirty thousand dollars. This cost does not include the price of manufacturing, transportation, and installation. Thus, for an increase of 1% in total neutron production compared to the

bare case, it would not be cost-efficient and provide significant technical benefits to ThESA goals.

Table 18. Cost table of the SS304 calculation for raw materials needed for the optimal reflector.

Total Volume Reflector	**Steel Density (g/cm^3)**	**Mass SS304 (kg)**	**Cost SS304 ($/kg)**	**Total Cost ($)**
7.55E+05	8.05	6.08E+03	4.87[37]	29605.23

6. SAFETY CALCULATIONS FOR OPERATION

6.1. Safety Introduction

ThESA is being designed and built for operation in one of the sub-basement peripheral rooms at the NSEC. ThESA is to be manned and operated by a two-person team. The ThESA design must then be so that it is safe to operate in a non-autonomous manner. The most crucial criterion for ThESA is that the radiation dose rate at locations with human access shall be less than the regulatory limits. It is also equally important to ensure that the room adjacent to ThESA is not at risk of radiation exposure beyond regulatory limits. Additionally, the FLiBe-Th pile never reach criticality, producing excessive neutron and gamma radiation.

6.2. Updated Design and Neutron Source Geometry Change

At this point, the mechanical team had been made aware that a reflector would not be beneficial to ThESA and matured the physical pool assembly design. Additional information from several components manufacturers at this point caused several design changes. The interior vessel would be made of SS316L to ensure maximum corrosion resistivity to the FLiBe-Th salt. The heaters are shown in light blue in Figure 34. The heaters also had temperature limitations and could not physically contact the primary vessel in red. Thus, the heaters had to be spaced several cms away from the primary vessel. Heaters were also placed at the bottom of the core to ensure distributed heating maximizing salt melt. Additional information and a thermal-mechanics study about the neutron generator revealed that having the generator within the primary vessel would be

impossible. The temperature of the generator would exceed its operational limitations if it were inside the primary vessel. It would also be easier to shield the room with the generator below the core instead of the top. The neutron generator moved from position 1 to position 2, shown in Figure 34. The change in position would enable greater ease of maintenance and less obstruction concerning the generator. The generator's original position was perfect as its solid angle opened up directly into the pool. Although better suited to ensure correct operating temperatures, the new location proved from a neutronics perspective inferior. The neutron generator's new position would safely ensure that operation without risk to the device. Table 19 shows there is a large neutron drop associated with the newest location of the neutron generator.

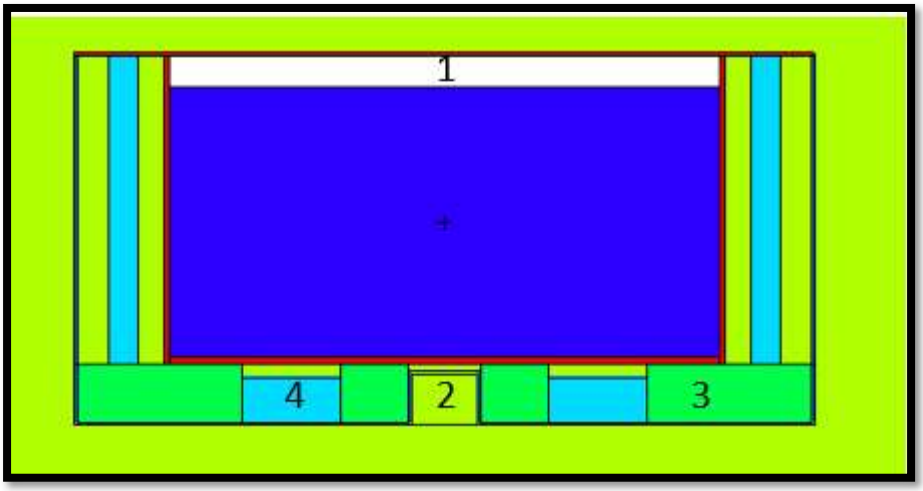

Figure 34. The updated ThESA core design at the time of the safety analyses post reflector studies.

Table 19. ThESA neutronics with the incorporated firebricks, heaters, and airgaps.

Location	k-eff	Relative Error	Total Fission Rate (neu/s)	Standard Deviation (neu/s)
2	0.01192	0.00001	1.39E+06	4.17E+02
1	0.01201	0.00001	2.42E+06	2.42E+02

6.3. MCNP Model of Entire ThESA Room with Radiation Shielding

The ThESA FLiBe assembly is driven with an external DD neutron source aimed at the pool assembly from underneath shown in Figure 34 at location 2. ThESA must have the capability to be operated from outside of the experimental room (102) shown in Figure 35. There is also an adjacent room (103) to the left of the experimental space that must be analyzed to ensure a safe working environment, specifically from a radiation exposure perspective. Additionally, a third location directly above the assembly was analyzed to ensure the radiation dose rate in all directions. The three locations shown in blue in Figure 35 are the points of interest in the radiation dose rate assessment for ThESA. The regulatory limit set by the Code of Federal Regulations (10 CFR Part 20) establishes that the total effective annual dose equivalent for the whole body be no more than 5,000 mrem radiation workers.[38]

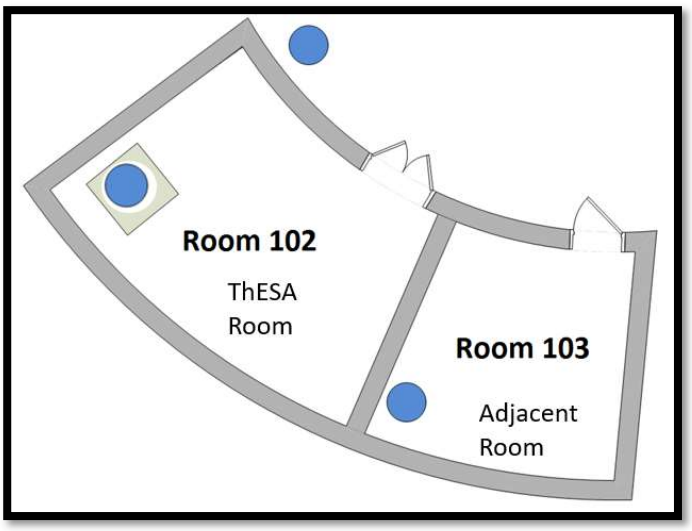

Figure 35. Diagram of the lab space orientation that encompasses the ThESA experiment and the adjacent room of interest.

Figure 36. was constructed in Solidworks using dimensions in cms gathered from the NSEC by a tape-measure and from a previous student work there. The room was constructed in Solidworks to ensure the MCNP input construction was modeled accurately. The only features not modeled in MCNP are the door and cube of concrete that sticks out of the wall. The concrete cube would be in the bottom right corner of Figure 36 between the water shield and concrete.

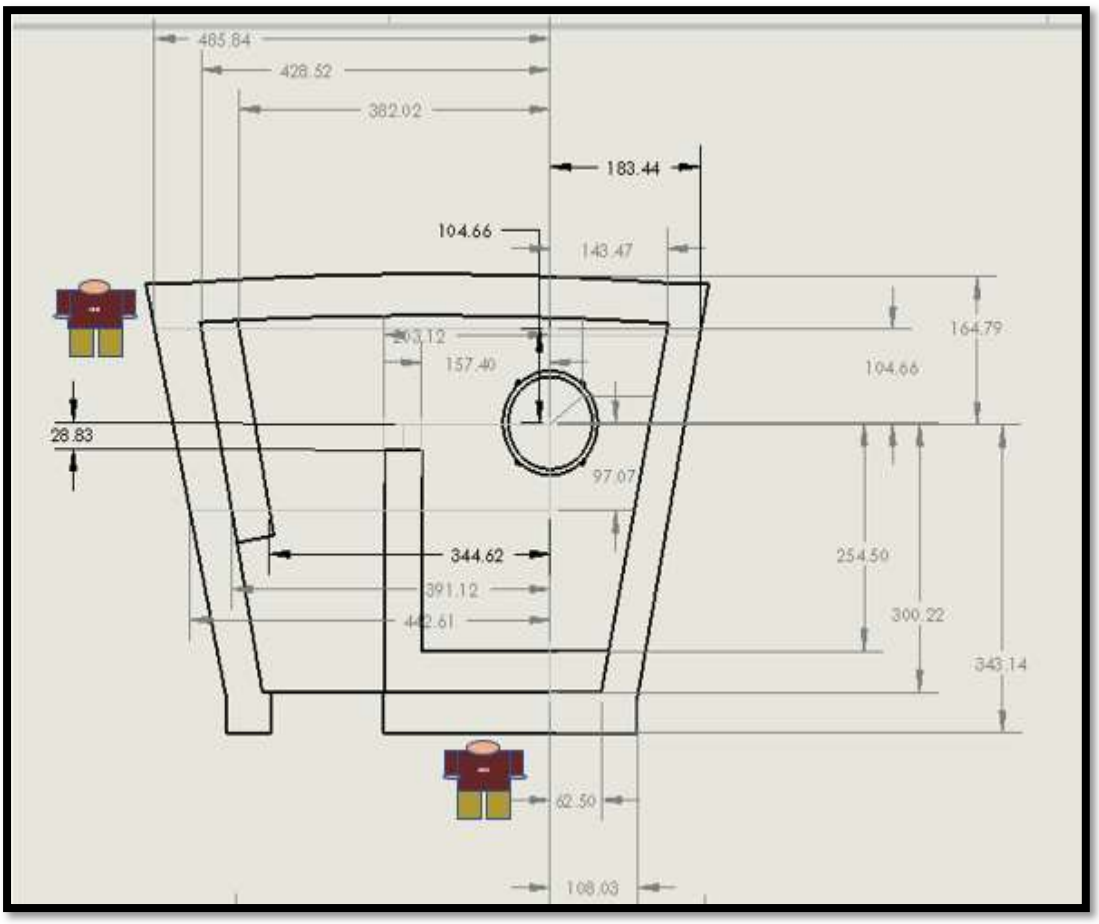

Figure 36. Schematics of the ThESA experiment room in cms with the core (circle) and the two locations of interest with the human cartoons.

Concrete and a slit 1cm wide replaced the door to simplify the model. The slit would simulate the neutron streaming through the edges of the door. Figure 37 shows the slit filled with air towards the bottom left and surrounded on two sides with concrete. The concrete block in the interior corner of the room replaced a water block. Figure 37

also shows the two locations where human beings would occupy during regular operation. The first human cartoon in the top left corner represents where someone in the adjacent room would be working. The second human cartoon represents where the human operating the control console for ThESA would be.

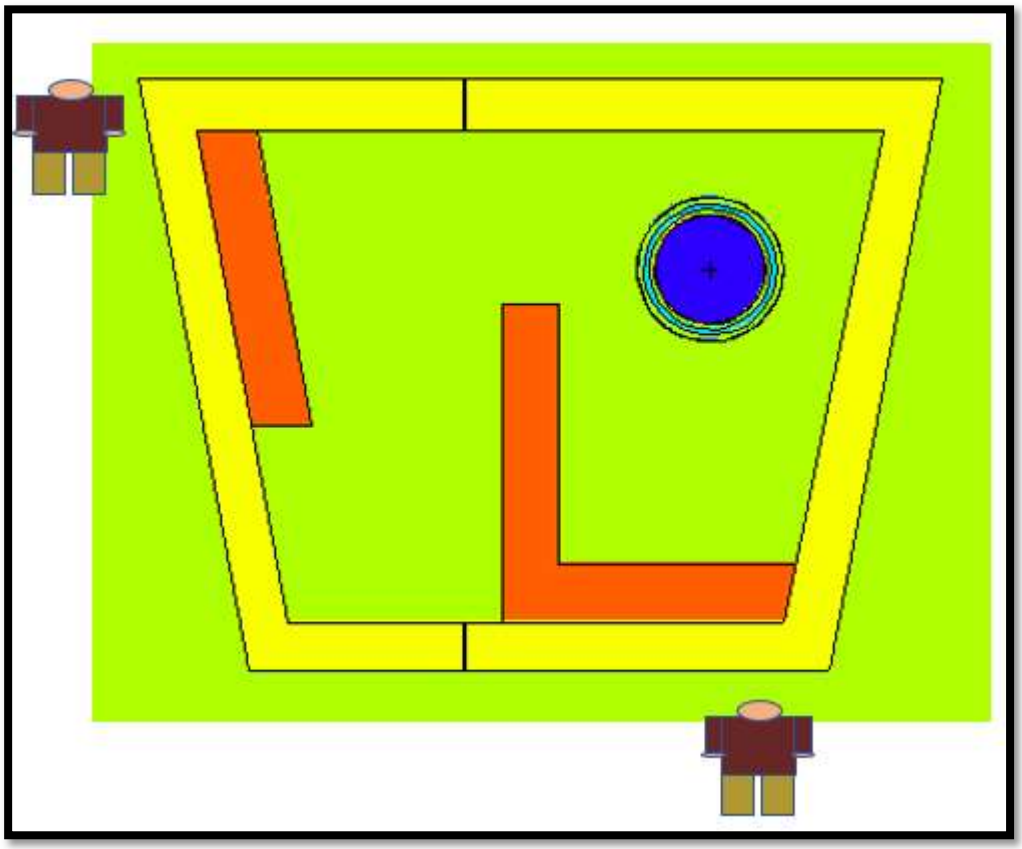

Figure 37. The room and pool assembly modeled in MCNP and visualized in Vised.

A combination of F5 radiation flux at a point (using MCNP F5 tallies) and flux-to-dose conversion factors were used to ensure the radiation dose rate at critical locations were below the regulatory limits. The F5 tallies, unlike F4 tallies, don't require particle histories to traverse a volume. Every particle collision within the environment is transported analytically towards the sphere of interest or tally. To convert the flux into usable dose rate, biological dose equivalent rate factors were used with the DE and DF feature of MCNP to convert from flux to dose rate in rem/h. The DE and DF features allow a piecewise dose-response function to be applied to specified radiation fluxes obtained in energy groups. The energy groups and dose rate response functions were extracted from the American National Standard ANSI/ANS-6.1.1-1977 and were used to calculate the radiation dose rates.

The dose rates calculated are shown in Table 20 for all critical locations using the radiation flux to dose rate-conversions and were found to be below the regulatory limit of 5000 mRem/year. The highest dose rate encountered was in an unoccupied location. The unoccupied was located inside the ground as the room was surrounded by dirt on that side. Thus, ThESA should be safe to operate as long as the experimental room is empty while the neutron generator is in operation.

Table 20. The radiation dose at critical locations around the ThESA experiment.

Location	Location Description	Total dose (mRem/Year)	Uncertainty (mRem/Year)
1	Control Console Location	2.64E+01	8.57E-01
2	Adjacent Room	1.73E+01	8.30E-01
3	Above Ceiling over the Core	4.89E+02	5.59E-02

6.4. Criticality Calculations

A primary concern for nuclear systems is the possibility that through either a swift change in geometric or material properties, the system will reach a critical or supercritical configuration. If a system rapidly changes to this configuration, a neutron or photon burst may occur, causing acute radiation exposure. This behavior can be typical of fissile material in solution. Typically, through some means, the fissile material could undergo neutron reactions with moderated neutrons leading to an undesired criticality configuration. This phenomenon is most common for uranium solutions because uranium-235 can fission with moderated neutrons, while thorium-232 cannot, as seen in Figure 38.

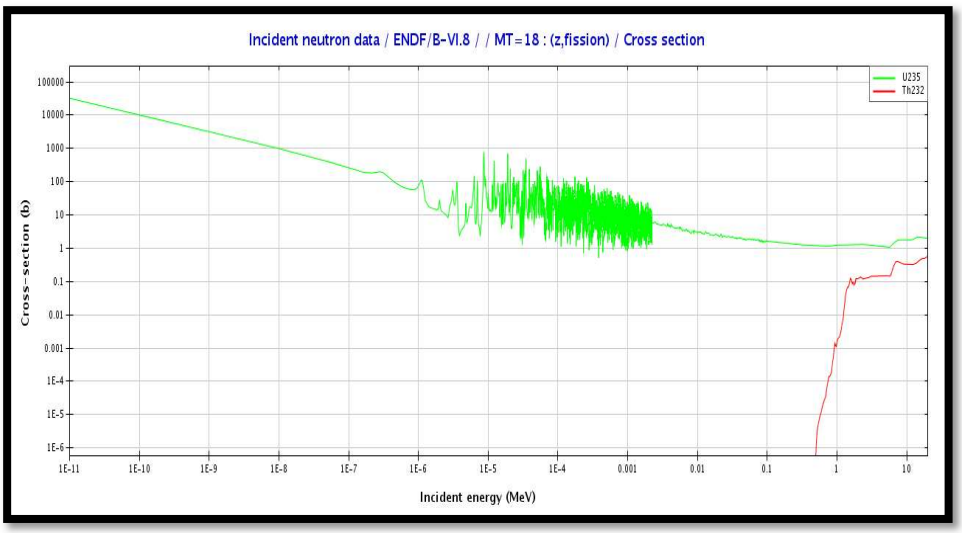

Figure 38. The fission cross-section of uranium-235 and thorium-232 (Janis, 2020).[40]

The k-inf value for the pool design was 0.01288, shown in Table 16. Thus, it can be assumed that no moderation or reflection can cause ThESA to go critical or supercritical. However, a test examination was performed to ensure the safety of those operating ThESA. Figure 39 shows in orange where the water would be if the entire room flooded. The system has only fertile fuel, and previous k-inf tests had calculated the system could only reach a maximum k-eff of 0.01288 with this pool configuration. With this configuration, the k-eff determined was 0.01192. Thus, it is safe to assume that even surrounded by water to act as a moderator, and there will not be sufficient thermal neutrons to induce the production of uranium-233 to cause a criticality accident. The

pool assembly simply does not contain enough fissile material to induce a super-criticality event.

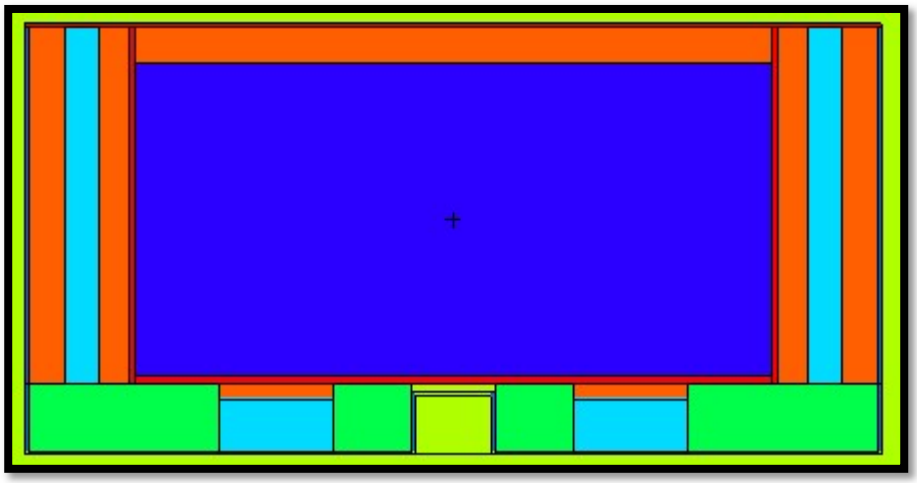

Figure 39. ThESA core with the primary and secondary vessel air gaps filled with water (orange).

6.5. Uranium-233 and Tritium Production

Thorium has the advantage of having the capability to produce uranium-233 in a thermal neutron environment. It is unique among the actinides in its ability to so. Thus, to alleviate proliferation concerns, a burnup calculation was carried out using MCNP to calculate the uranium-233 production rate. ThESA inherently has a fast neutron spectrum, although neutrons will moderate to some degree. Time-steps of 30 days were used with the neutron source at maximum power. The power was calculated by taking

the total neutrons produced and backward-calculating the energy emitted per second. The simulation was set to run over an entire year at full power continuously. Though, the experiment would operate on the order of several weeks, not months. Thus, the simulation considered is a conservative estimate as there are physical limitations on how long the neutron generator can operate. Figure 40 shown is the linear increase of uranium-233 production as a function of time. Even over an entire year, the total amount of uranium-233 would still be less than a milligram.

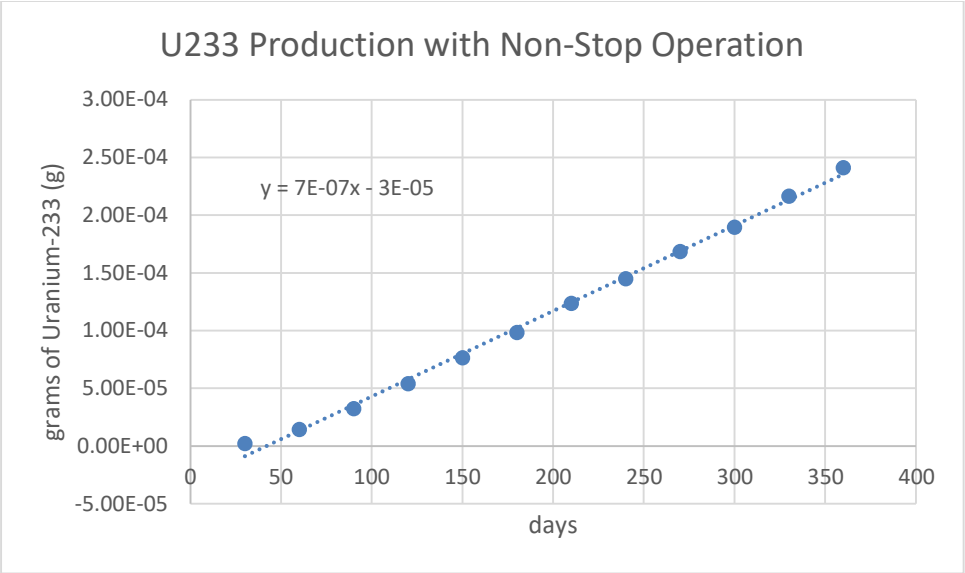

Figure 40. The uranium-233 production in grams as a function of time at full power.

Alongside the production of uranium-233, there was also a concern with the lithium-6 in the FLiBe mixture transmuting into tritium. Tritium is of concern due to its crucial role in nuclear fusion in weapons. Thus, using an F4 averaged track length flux estimation (F4 tally in MCNP) and ENDF reaction number 105 (n, H_3), the reaction rate for tritium production was calculated over the entire core. The tally estimated the atoms of tritium produced on average over the entire pool assembly. Using the Avogadro number and different time periods, the moles of tritium produced are shown in Table 21. The system simply does moderate neutrons to produce any significant quantities of tritium.

Table 21. The production tritium in moles as a function of time.

Time	Tritium (moles)	Standard Deviation (moles)
1 Minute	1.40E-19	6.69E-21
1 Hour	8.40E-18	4.02E-19
1 Day	2.02E-16	9.64E-18
1 Week	1.41E-15	6.75E-17
1 Month	5.65E-15	2.70E-16
3 Months	1.69E-14	8.10E-16
1 Year	6.78E-14	3.24E-15

7. CONCLUSION AND FUTURE WORK

7.1. Final Design Analyses

After completion of the safety analysis, the mechanical engineering team added steel inserts to ThESA. The most significant difference from the core used in the safety analysis and the one shown in Figure 41 was the addition of stainless-steel inserts for scientific instrumentation. The simplification is the exclusion of helix style pipe and some minor pipes used for thermal couples. This helix pipe was not possible to model in MCNP without relative ease. The pipes seen in Figure 41 in red did not significantly decrease the k-eff value when introduced into the model. Thus, the exclusion of the helix and the smaller thermocouple inserts should have minimal consequences on ThESA. Figure 42 shows a more detailed view of the entire pipe instrumentation.

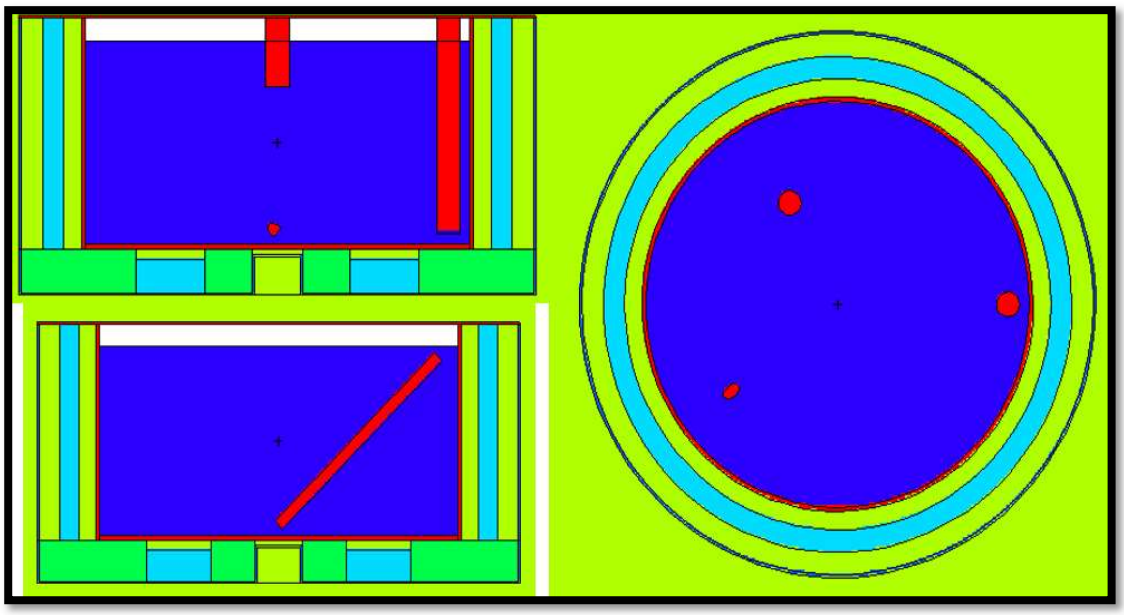

Figure 41. Final ThESA MCNP assembly design with the inclusion of the major in-core piping for scientific instrumentation.

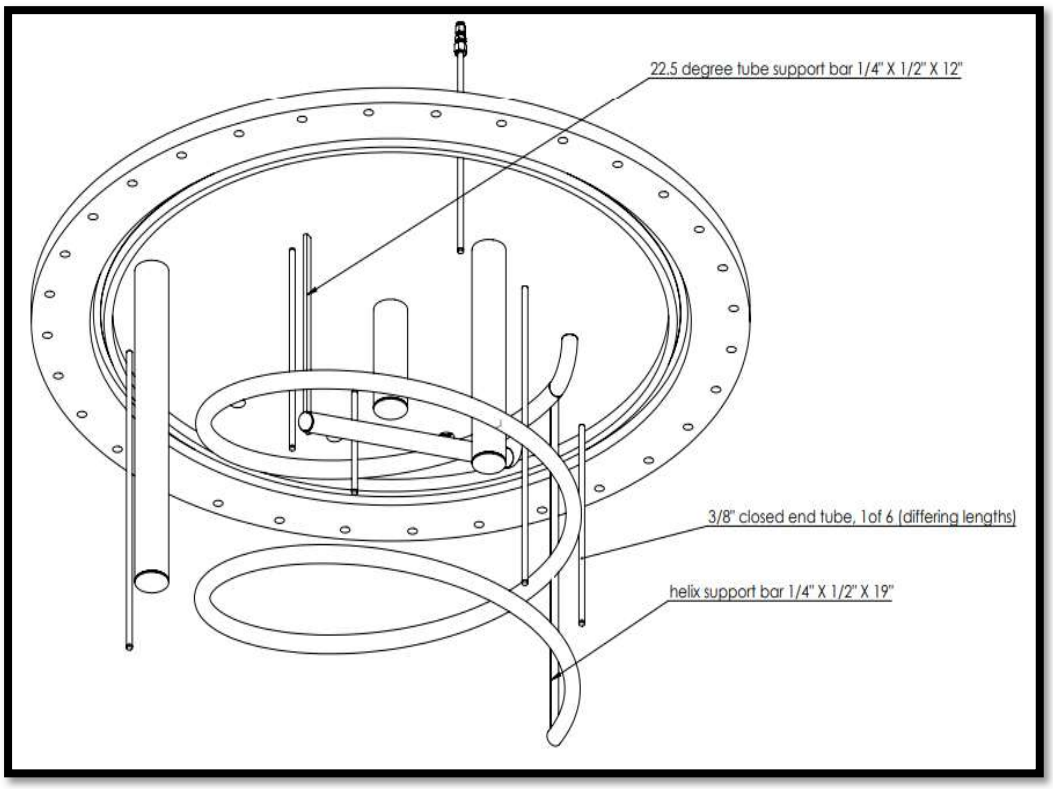

Figure 42. The mechanical design of the top lid, including the pipes used for scientific equipment.

7.1.1. Effects on Neutronics Results with Addition of Accessory Equipment

The results with the addition of the accessories pipes, the k-eff, and the total neutron population were affected, but the results were similar, although statistically different. Table 22 shows the results on k-eff and the total neutron population with the final design.

Table 22. The neutronics results of the most current ThESA design.

k-eff	Standard Deviation	Total Fission Rate (neu/s)	Standard Deviation (neu/s)
0.01189	0.00001	1.38E+06	2.76E+02

It is necessary to be able to differentiate between source neutrons and fission neutrons. The neutron source generator produces neutrons with energies 2-3 MeV. Figure 43 shows the fission distribution of uranium-235 and thorium-232. Since the two energy distributions are similar using the Watt distribution of the neutron spectrum for uranium-235, the fraction of fission neutrons born from thorium can be deduced. The fraction of fission neutrons is obtained by integrating over the Watt spectrum and calculating the probability of neutrons born from 0 eV to 3 MeV shown in Equation 13.[39] Then that probability is subtracted from 1.0 to calculate the fraction of neutrons born above energy 3.0 MeV in Equation 14. The probability P_2 can then be used to calculate the total neutrons born with energies above 3.0 MeV shown in Equation 15.

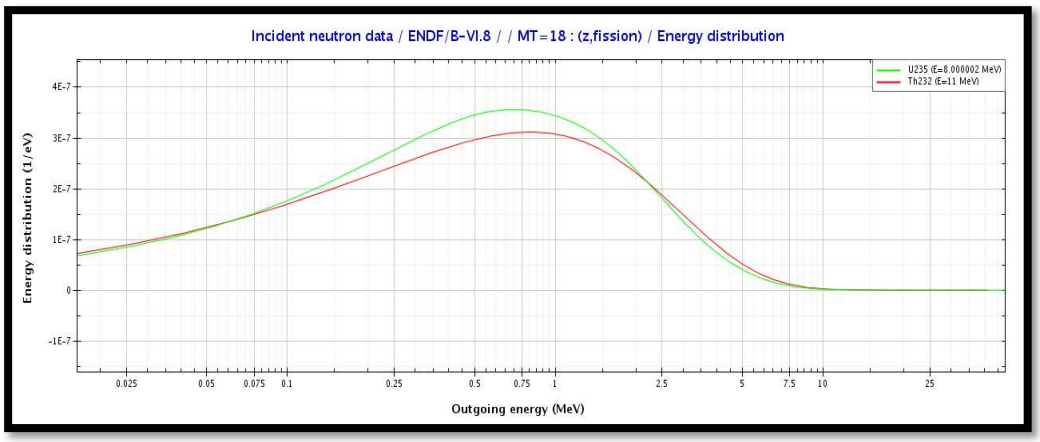

Figure 43. Fission neutron energy distribution of uranium-235(green) and thorium-232(red) (Janis, 2020).[41]

$$P_1 = \int_{0\ eV}^{3\ MeV} 0.4865 \sinh\left(\sqrt{2E}\right) e^{-E}\, dE = 0.791789 \qquad \text{Eq.(13)}$$

$$P_2 = 1.0 - 0.711201 = 0.208211 \qquad \text{Eq.(14)}$$

$$DN = ToTNeu * P_2 = 2.87E5 \qquad \text{Eq.(15)}$$

Where:

$P1$: The probability of neutrons born between energies 0 eV to 3MeV.

$P2$: The probability of neutrons born between energies from 3MeV to 20 MeV.

DN: The total number of differentiable thorium fission neutrons with energies above 3 MeV.

TN: Total number of thorium fission neutrons of all energies.

7.2. Conclusion

The neutronics analyses described in the document successfully supported the design of an external neutron driven subcritical thorium assembly. The work performed included a neutronics comparison study of a pin-type and pool-type assembly of FLiBe-Th, a parametric reflector study, and a safety analysis. The comparison study results indicated that the pool-type would be a better configuration considering the pin-type operational and manufacturing limitations. The parametric reflection study results indicated that the system was prone to leakage, and the benefits of a reflector did not justify the cost. The safety analysis revealed no significant hazards or scenarios for operators. The radiation dose rates at critical locations were below operational, regulatory limits. The system would not produce any significant quantities of either tritium or uranium-233. Also, the system could not reach criticality given any existing materials or geometric configuration. After the mechanical engineering team completed the final design, the final analysis revealed that the total number of detectable neutrons per second over the entire assembly was 2.87E5 +/- 5.75E+01. The detectable neutrons are those that had energies of 3.0 MeV or above. The goal of ThESA was to produce an environment where thorium could efficiently fission, and as of the latest simulations, should undoubtedly do so.

7.3. Potential Future Work

Thorium is the actinide with the least amount of operational experience as an alternative nuclear fuel. The lack of experience is simply due to the dominance of

uranium systems in the early 20th century. ThESA allows for experimental observation of Th-232 fissioning in a fast spectrum. Thus, the ThESA environment will enable the collection and data acquisition of valuable nuclear properties of Thorium-232. Potential experiments include validating the delayed neutron precursor groups and validating thorium reaction rates.

7.3.1. Thorium Delayed Neutron Precursors Study

It is valuable to understand the delayed neutron spectrum following the fast fission of thorium-232 in molten salt. The delayed neutrons aid the reactor into a delayed-critical configuration. Delayed-critical is when the system's k-eff is only above 1.0 with the inclusion of the delayed neutrons. If a reactor were prompt-critical, it would be uncontrollable by external methods.[42] A potential methodology to validate thorium-232 delayed neutron groups using the ThESA experiment is shown below:

1. Ensure ThESA is externally powered for a few hours
2. Insert a neutron detector (does not have to differentiate between neutron energy levels)
3. Set count rate at varying lengths; time lengths may have to be adjusted for the shortest and longest-lived delayed precursors
4. Use a generalized gradient nonlinear solver on exponential decay chart of the count rates to calculate the decay groups

7.3.2. Validation of Thorium Reaction Rates

ThESA may be capable of approximating (n,γ) and (n,f) reaction rates for thorium-232 using neutron activation analysis. The neutron activation analysis (NAA) technique involves inserting a material with specified neutron reactions with a specified energy range. Typical NAA uses cadmium to shield the gold from thermal neutrons and then compare it to a bare gold foil to simultaneously solve the thermal and epithermal flux.[43] However, the thermal and epithermal ranges in the ThESA would be dominated by DD source neutrons. Thus, a reaction is needed with a 3 MeV minimum energy limit to observe the fission spectrum's fast end. Figure 44 shows the sulfur-32 (z,p) reaction that would meet the neutron energy range appropriate to differentiate between the source and fission neutrons. By measuring the protons created from high energy neutron capture by sulfur-32, the neutrons above 3 MeV can be measured. Thus, if sulfur-32 is activated predominantly from fission neutrons, it will simplify the neutron differentiation between the source and fission events. If the proton energy can be correlated to the fission neutron energy, it may help identify the fission neutron spectrum's fast end. This fast end of the fission spectrum could then be used to extrapolate the rest of the spectrum backward.

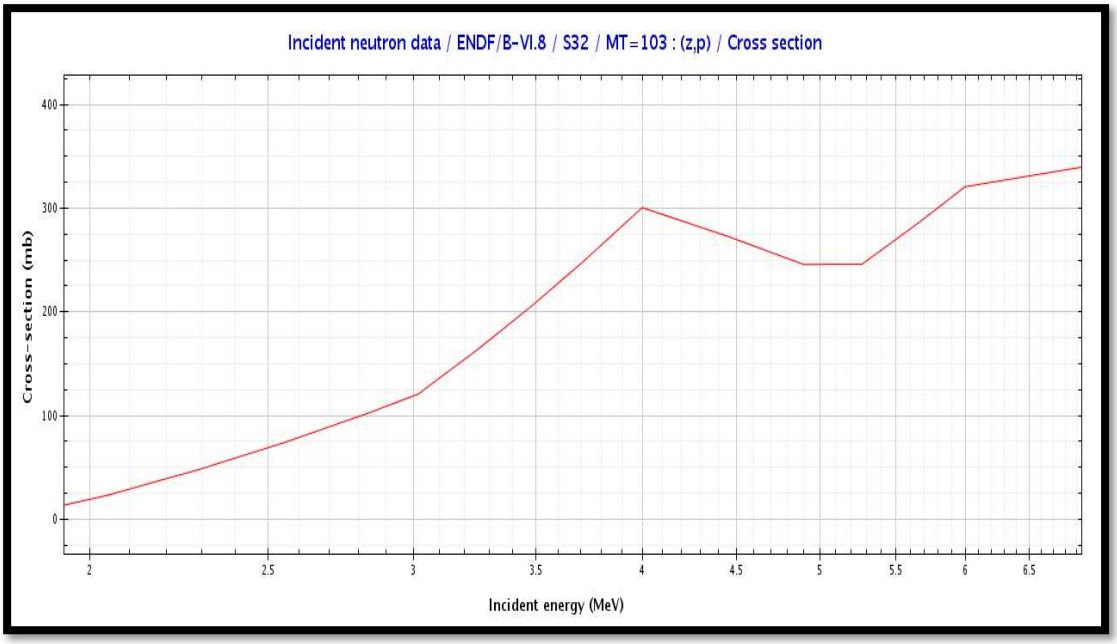

Figure 44. The (z,p) reaction may help observe the higher end of the fission spectrum of thorium-232 (Janis, 2020).[44]

REFERENCES

1.private communication, Yassin Hassan, Texas A&M University (2018).

2.Aufiero, M., Cammi, A., Fiorina, C., Leppänen, J., Luzzi, L., & Ricotti, M. E. (2013). An extended version of the SERPENT-2 code to investigate fuel burn-up and core material evolution of the Molten Salt Fast Reactor. *Journal of Nuclear Materials*, *441*(1-3), 473-486.

3.Belle, J., & Berman, R. M. (1984). *Thorium dioxide: properties and nuclear applications* (No. DOE/NE--0060). USDOE Assistant Secretary for Nuclear Energy.

4.McDeavitt, S. M., Xu, Y., Downar, T. J., & Solomon, A. A. (2007). Zirconium matrix cermet for a mixed uranium-thorium oxide fuel in an SBWR. *Nuclear technology*, *157*(1), 37-52.

5.Van Gosen, B. S., Gillerman, V. S., & Armbrustmacher, T. J. (2009). *Thorium Deposits of the United States-Energy Resources for the Future?* (No. 1336). US Geological Survey.

6.Belle, J., & Berman, R. M. (1984). *Thorium dioxide: properties and nuclear applications* (No. DOE/NE--0060). USDOE Assistant Secretary for Nuclear Energy.

7.Heuer, D., Merle-Lucotte, E., Allibert, M., Brovchenko, M., Ghetta, V., & Rubiolo, P. (2014). Towards the thorium fuel cycle with molten salt fast reactors. *Annals of Nuclear Energy*, *64*, 421-429.

8.Herring, J. S., MacDonald, P. E., Weaver, K. D., & Kullberg, C. (2001). Low cost, proliferation resistant, uranium–thorium dioxide fuels for light water reactors. *Nuclear engineering and design*, *203*(1), 65-85.

9.Hargraves, R., & Moir, R. (2010). Liquid Fluoride Thorium Reactors: An old idea in nuclear power gets reexamined. *American Scientist*, *98*(4), 304-313.

10.reprinted from de Kageneck, A., & Pinel, C. (1998). The Joint Convention on the Safety of Spent Fuel Management and on the Safety of Radioactive Waste Management. *The International and Comparative Law Quarterly*, *47*(2), 409-425.

11.reprinted from Colonna, N., Belloni, F., Berthoumieux, E., Calviani, M., Domingo-Pardo, C., Guerrero, C., ... & Plag, R. (2010). Advanced nuclear energy systems and the need of accurate nuclear data: the n_TOF project at CERN. *Energy & Environmental Science*, *3*(12), 1910-1917.

12.reprinted from Juhasz, A., Rarick, R., & Rangarajan, R. (2009, August). High efficiency nuclear power plants using liquid fluoride thorium reactor technology. In *7th International Energy Conversion Engineering Conference* (p. 4565).

13.Gehin, J. C. (2015). History of the ORNL Molten Salt Program. *Oak Ridge National Laboratories*, *15*(10).

14.reprinted from Ergen, W. K., Callihan, A. D., Mills, C. B., & Scott, D. (1957). The Aircraft Reactor Experiment—Physics. *Nuclear Science and Engineering*, *2*(6), 826-840.

15.MacPherson, H. G. (1985). The molten salt reactor adventure. *Nuclear Science and engineering*, *90*(4), 374-380.

16.reprinted from Haubenreich, P. N., & Engel, J. R. (1970). Experience with the molten-salt reactor experiment. *Nuclear Applications and technology*, *8*(2), 118-136.

17.reprinted from Glass, Jarrod, Anthony Burgess, and Takuya Okugawa. "Investigation of thermodynamic factors influencing Thorium reactor efficiencies." *PAM Review* 2 (2015): 14-31.

18.Bowman, C. D. (1998). Accelerator-driven systems for nuclear waste transmutation. *Annual Review of Nuclear and Particle Science*, *48*(1), 505-556.

19.Barros, G. D. P., Pereira, C., Veloso, M. A., & Costa, A. L. (2012). Study of an ADS loaded with thorium and reprocessed fuel. *Science and Technology of Nuclear Installations*, *2012*.

20.Molten Salt Reactors. (2018, December 1). Retrieved October 01, 2020, from https://www.world-nuclear.org/information-library/current-and-future-generation/thorium.aspx

21.Cheatham III, J. R., Cisneros, A. T., Latkowski, J. F., Vollmer, J. M., & Johns, C. J. (2019). *U.S. Patent No. 10,438,705*. Washington, DC: U.S. Patent and Trademark Office.

22.Reprinted from *TerraPower Technology Page*. (n.d.). doi:https://www.terrapower.com/our-work/molten-chloride-fast-reactor-technology/

23.Choe, J., Ivanova, M., LeBlanc, D., Mohaptra, S., & Robinson, R. (2018). Fuel Cycle Flexibility of Terrestrial Energy's Integral Molten Salt Reactor (IMSR). In *38th Annual Conference of the Canadian Nuclear Society and 42nd Annual CNS/CNA Student Conference, Saskatoon, SK, Canada, June* (pp. 3-6).

24.reprinted from Choe, J., Ivanova, M., LeBlanc, D., Mohaptra, S., & Robinson, R. (2018). Fuel Cycle Flexibility of Terrestrial Energy's Integral Molten Salt Reactor

(IMSR). In *38th Annual Conference of the Canadian Nuclear Society and 42nd Annual CNS/CNA Student Conference, Saskatoon, SK, Canada, June* (pp. 3-6).

25.Krepel, J. (2015). SAMOFAR-a paradigm shift in reactor safety with the molten salt fast reactor. In *Proceedings of the international thorium energy conference: gateway to thorium energy*.

26.Booth, T. E. (1985). *Sample problem for variance reduction in MCNP* (No. LA-10363-MS). Los Alamos National Lab., NM (USA).

27.reprinted from NGEN 400 Description. (2019). Retrieved October 22, 2020, from http://www.starfireindustries.com/uploads/2/2/1/1/22111816/datasheet_ngen-400_rev01-19.pdf

28.Six factor formula. (2020, June 10). Retrieved October 11, 2020, from https://en.wikipedia.org/wiki/Six_factor_formula

29.Brown, F. B. (2010, October). "K-effective of the World" and Other Concerns for Monte Carlo Eigenvalue Calculations. Retrieved October 01, 2020, from https://mcnp.lanl.gov/pdf_files/la-ur-10-06874.pdf

30.MCNP Manual 6.2. (n.d.). In *MCNP Manual 6.2* (6.2 ed., pp. 3-7). LANL.

31.MCNP Manual 6.2. (n.d.). In *MCNP Manual 6.2* (6.2 ed., pp. 3-124, Note 2). LANL.

32.reprinted from Janis Th232 fission and absorption20 cross section. (2020). Retrieved October 01, 2020, from https://www.oecd-nea.org/janisweb/renderer/2334

33.Chirayath, S., Dr. (2020, March 01). Reflector Thickness [Personal interview].

34.Herman, M., & Trkov, A. (2009). ENDF-6 Formats Manual. Retrieved October 01, 2020, from https://www.bnl.gov/isd/documents/70393.pdf Table 14: ENDF sum rules for cross-sections

35.Reflector Savings, Diffusion Theory. (2001). Retrieved October 01, 2020, from https://www.nuclear-power.net/nuclear-power/reactor-physics/neutron-diffusion-theory/reflector-savings/

36.Tahara, Y., Sekimoto, H., & Miyoshi, Y. (2001). Reactivity Effect of Iron Reflector in LWR Cores. *Journal of Nuclear Science and Technology, 38*(2), 102-111. doi:10.1080/18811248.2001.9715012

37.Stainless Steel 304 price per kg. (n.d.). Retrieved October 11, 2020, from https://www.stindia.com/stainless-steel-304-316l-price-per-kg-india.html

38.NRC Regulations (10 CFR) PART 20—STANDARDS FOR PROTECTION AGAINST RADIATION. (1991, May 21). Retrieved October 01, 2020, from https://www.nrc.gov/reading-rm/doc-collections/cfr/part020/

39.Grundl, J. (1971, October 31). FISSION-NEUTRON SPECTRA: MACROSCOPIC AND INTEGRAL RESULTS. Retrieved October 01, 2020, from https://www.osti.gov/servlets/purl/4754459

40.reprinted from Janis Th232 fission and U235 fission cross section. (2020). Retrieved October 09, 2020, from https://www.oecd-nea.org/janisweb/renderer/17

41.reprinted from Janis Th232 fission and absorption20 cross section. (2020). Retrieved October 01, 2020, from https://www.oecd-nea.org/janisweb/renderer/2334

42. Wilkins Jr, J. E. (1959). The behavior of a reactor at prompt critical when the reactivity is a linear function of time. *Nuclear Science and Engineering*, *5*(4), 207-214.

43. Osae, E., Nyarko, B., Serfor-Armah, Y., & Akaho, E. (1998). An alternative method for the measurement of thermal neutron flux (modified cadmium ratio method). *Journal of radioanalytical and nuclear chemistry*, *238*(1-2), 105-110.

44. reprinted from Janis Incident neutron data for sulphur-32. (n.d.). Retrieved from https://www.oecd-nea.org/janisweb/renderer/3936

APPENDIX A

MATERIAL CARDS USED FOR MCNP

```
c FLiBe-Th Materials
m1    3007.82c       -0.0416
      4009.82c       -0.0278 90232.82c       -0.5268 9019.82c       -0.4037
c Stainless Steel Heated Interior Calculations/Materials/ 7.92g/cc
m2    24050.80c    0.00071866  $Stainless Steel 304
      24052.80c     0.013859 24053.80c     0.0015715 24054.80c    0.00039117
      26054.80c     0.0037005 26056.80c       0.05809 26057.80c     0.0013415
      26058.80c    0.00017853 28058.80c     0.0044318 28060.80c     0.0017071
      28061.80c   7.4207e-005 28062.80c    0.00023661 28064.80c   6.0256e-005
c Ceramic Heater  Calculations/Materials/Ceramic_Heater 0.28g/cc
m3    13027.82c     0.106933 26056.82c 0.005444
      08016.82c     0.648845 14028.82c 0.238779
c FireBrick Assuming 23%Alumina 73%Silica
m4    13027.82c     0.108708   $ Ceramic Material 0.28g/cc
      08016.82c     0.648549
      14028.82c     0.242743
c Unheated Stainless Steel Heated Interior Calculations/Materials/ 7.92g/cc
m5    24050.81c    0.00071866
      24052.81c     0.013859 24053.81c     0.0015715 24054.81c    0.00039117
```

26054.81c 0.0037005 26056.81c 0.05809 26057.81c 0.0013415

26058.81c 0.00017853 28058.81c 0.0044318 28060.81c 0.0017071

28061.81c 7.4207e-005 28062.81c 0.00023661 28064.81c 6.0256e-005

c Air Materials Compendium 0.001205 g/cm^3 Materials Compd. Pg 1(Air,near sea level)

m6 6000 0.000150 7014 0.784437

8016 0.210750 18000 0.004671

c Concrete Material Pg.12 Better Materials Compendium Density 2.30g/cm^3

m7 1001 0.304245

6012 0.002870

8016 0.498628

11023 0.009179

12000 0.000717

13027 0.010261

14000 0.150505

19000 0.007114

20000 0.014882

26000 0.001599

c Borated Water 5% Allen Calculation Materials/BoratedWater 1.0 g/cm^3

m8 5011.81c 4.93E-03

8016.81c 3.37E-01

1001.81c 6.58E-01

```
m9 1001 2 08016 1
m10  14000.82c -0.010 $ Si Stainless Steel 316 pg 100 7.92g/cc
     24000.82c -0.170 $ Cr
     25055.82c -0.020 $ Mn
     26000.82c -0.655 $ Fe
     28000.82c -0.120 $ Ni
     42000.82c -0.025 $ Mo
```